

# **Geophysical Surveys in the Harshaw Creek Area, Patagonia Mountains, Arizona**

**Field Studies in Geophysics 2024**

Laboratory for Advanced Subsurface Imaging LASI-24-1

May 2024

Layan Alziyadi, Lindsey Frenia,

Bridgett Holman, Hannah Mo,

Cole Stokes, Angela Tatsch,

Dr. Ben K. Sternberg

## **Abstract**

On February 10, 2024, and March 2–3, 2024, three geophysical surveys were conducted by students at the University of Arizona and members of the United States Geological Survey. Each survey took place along the Patagonia Fault Zone just SE of the town of Patagonia, Arizona. Geophysical data were collected by using the direct-current resistivity method and a linear dipole-dipole and strong gradient array setup. The objective of these surveys was to map the fault to understand the subsurface structural nature of faulting along a short segment of the S side of the basin and range structure. The results of the survey show the fault system is complex with multiple faults causing progressive down drops of highly resistive rocks, creating a graben. An understanding of the structural complexity was our main objective along the fault. Inversions of the resistivity data showed evidence of complex and subparallel faulting associated with high subbasins with interpretable water or wet sediments in zones away from what was described by geologists in previously published maps as a single fault. Inverted pseudosections from our surveys show areas of low resistivity within the graben edge that may be interpreted as saturated sediments, i.e., water storage areas. These results demonstrate that direct-current resistivity methods can reveal shallow subsurface structural configurations and potential water-bearing areas. This survey contributes to geologists' understanding of subsurface structural continuity, specifically within the Patagonia Fault zone. Additionally, this method can help both property owners and businesses make informed decisions about where and how deep to drill wells.

# Table of Contents

Acknowledgments.....	1
1 Introduction.....	2
1.1 Purpose and Scope .....	2
1.2 Previous Investigations .....	2
1.3 Project History .....	8
1.4 Geologic Background .....	10
1.4.1 Geology.....	10
1.4.2 Hydrology .....	10
1.5 Sites Description .....	10
2 Methods.....	15
2.1 Equipment and In-Field Setup .....	15
2.2 Data Processing Using AGI EarthImager 2D.....	17
2.3 Archie’s Equation .....	19
2.4 Test Site .....	19
3 Results and Interpretations.....	23
3.1 Line PB .....	24
3.2 Line PC .....	32
3.3 Line PD.....	37
4 Conclusions.....	46
4.1 Future work.....	47
5 Appendix.....	48
5.1 Misfit Scatter Plots.....	48
5.2 GeoDaze.....	50
5.3 Field Picture .....	52
6 References.....	53

## **Acknowledgments**

The University of Arizona Geophysics Field Studies class (GEOS 416) would like to thank the United States Geological Survey for providing funding and support for this project. Thank you to Jamie Macy, Jacob Conrad, and Floyd Gray with the USGS for the planning, guidance, data processing assistance, and access to equipment vital to this project. A special thank you to landowner Dave Martin, the landowners the Buchanans, Denise Bowdon of South32 Mine, and Mining Company South32. Thank you to the Coronado National Forest for access to the land.

# 1 Introduction

## 1.1 Purpose and Scope

The purpose of this report is to better understand the complex fault system in Patagonia and how groundwater flows in the Lower Harshaw Creek area, a region structurally defined by a basin and range graben and Patagonia Fault. Because well drill logs are limited, geophysical data are vital to characterizing structural features and bedding offset associated with fault movement. Mapping bedrock features helps us construct a conceptual model about preferential water pathways. Modeling includes water impediment, how water might flow across these areas, and where bedrock may be pushing water to the surface. In terms of the adjacent alluvial system, we seek to understand how much water can be contained along Harshaw Creek. How water flows across these different rock units and is chemically altered adds to our understanding of where dirty, mineral-rich water versus clean, potable water might be located. Our geophysical data will be utilized by the USGS and Nature Conservancy to also construct numerical groundwater models. Concerns in the town of Patagonia revolve around water being discharged from the aquifer system, largely by mining companies. Identifying excessive groundwater pumping helps interested groups analyze the impacts on local springs and ecosystems from aquifer dewatering.

## 1.2 Previous Investigations

Extensive research has been carried out to study the region of the Sonoita Creek basin due to the presence of a complex basin and range system. Menges (1981) conducted a series of gravity surveys as well as structural and stratigraphic analysis of the basin, which reveals the existence of a primary boundary fault of the Sonoita Creek Graben under the exposed fault traces. Within this area, the Patagonia Fault Zone (PFZ), which forms the SE boundary of the Patagonia sub graben (Figure 1.2-1).



The first-order residual gravity anomaly, which is supposed to represent the local density variation because of subsurface alluvial–bedrock interface configuration, after reduction from the gravity data (Figure 1.2-2). It is noted that all anomalies are negative, which may indicate the region has a mass deficiency or a partially compensated regional uplift. The contours display irregular and fragmented patterns, which seem to be influenced by nearby basin margins and exposed fault zones. In addition, these contours reveal secondary closed minima within the main anomaly low of the central Sonoita Creek basin. One of these minima is positioned centrally, while the other is shifted asymmetrically toward the SE border. This border coincides with a prominent linear region of steeply sloping anomaly contours that relate to the trace of the PFZ, suggesting that an underlying extension of this significant fault zone bounding the basin is present (Menges, 1981).

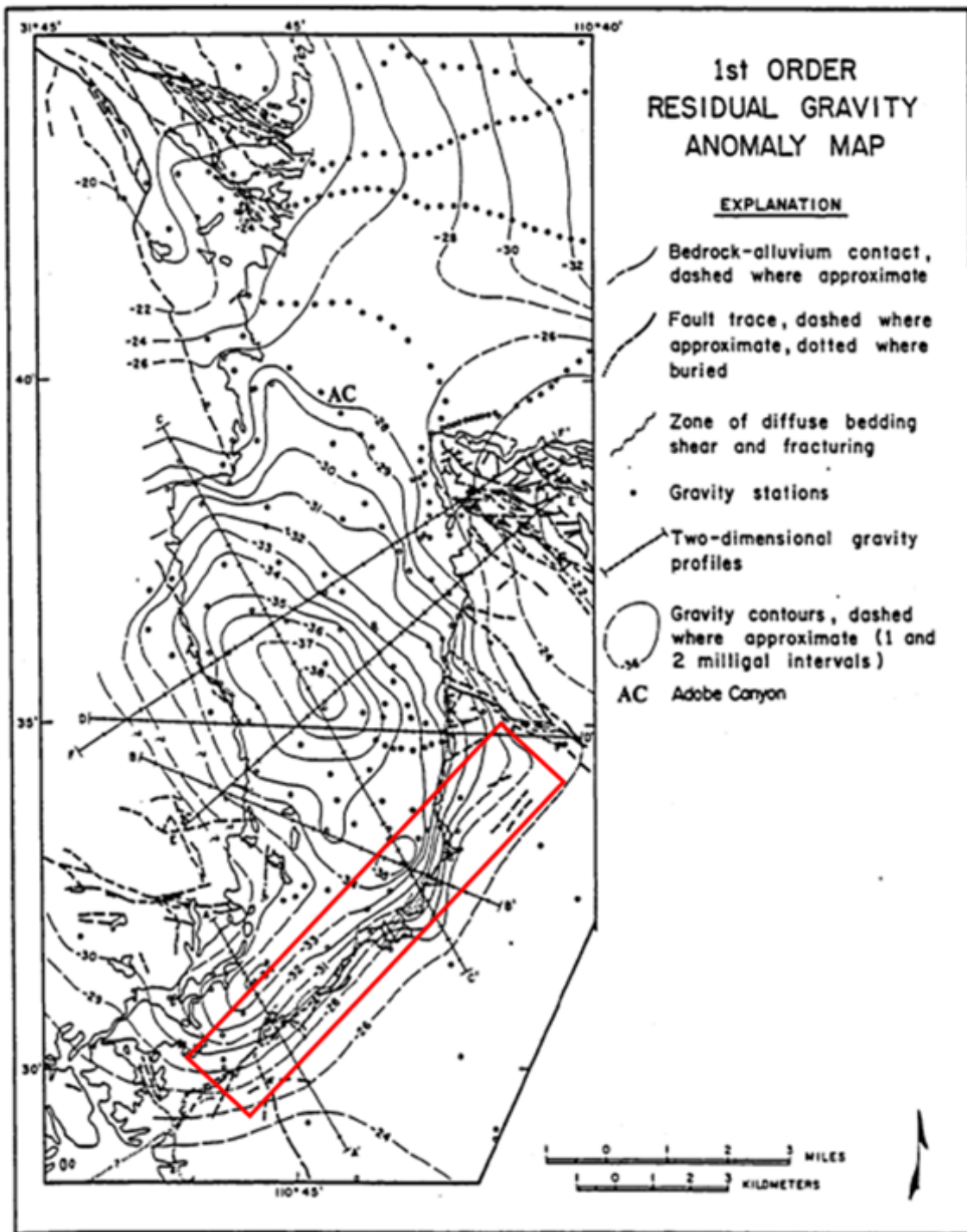


*Figure 1.2-2. First-order residual gravity anomaly map; the red box indicates a fault structure represented by steep-sloping anomalies (Menges, 1981).*

Vikre et al. (2014), intrigued by the porphyry deposits in response to hydrothermal alterations, investigated the Patagonia Mountain regions by utilizing geochemical analysis and geologic mapping (Figure 1.2-3). The primary structure in this area is the NW-striking Harshaw Creek fault, which is responsible for the displacement of over 3 km of stratigraphic layers. The exhumation of the PZ batholith, which does not include the porphyry Cu-Mo system, is associated with a secondary fault. A Three-R Shear Zone, presented in the NW of this batholith, is another indicator of the fault system. Furthermore, another fault, with a significant offset, has displaced Tertiary Quaternary colluvial deposits downward on the NW side of Red Mountain compared to the strongly altered volcanic rocks forming the mountain (Menges, 1981). These structures imply the existence of a deep crust structure (Vikre et al., 2014).

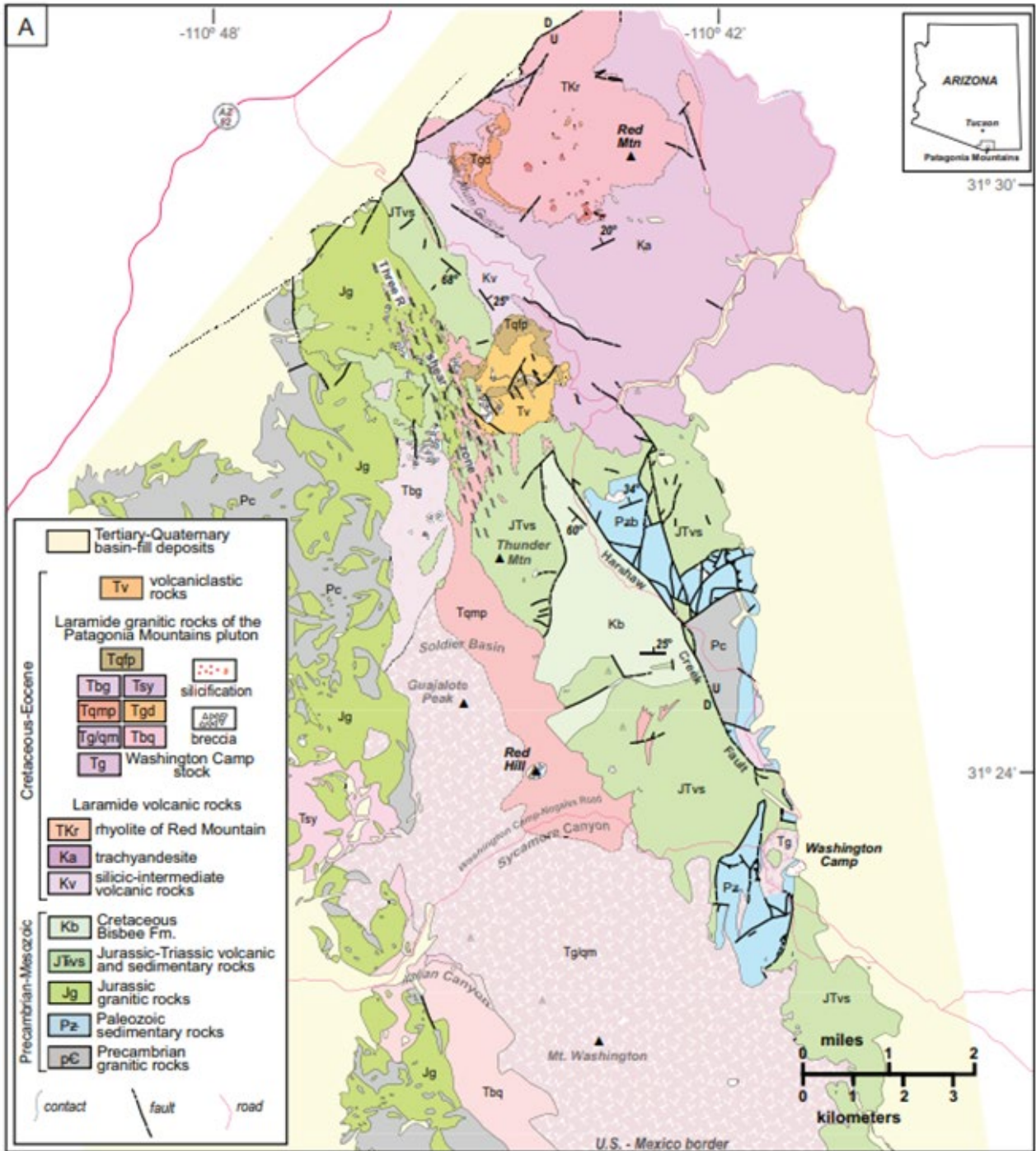
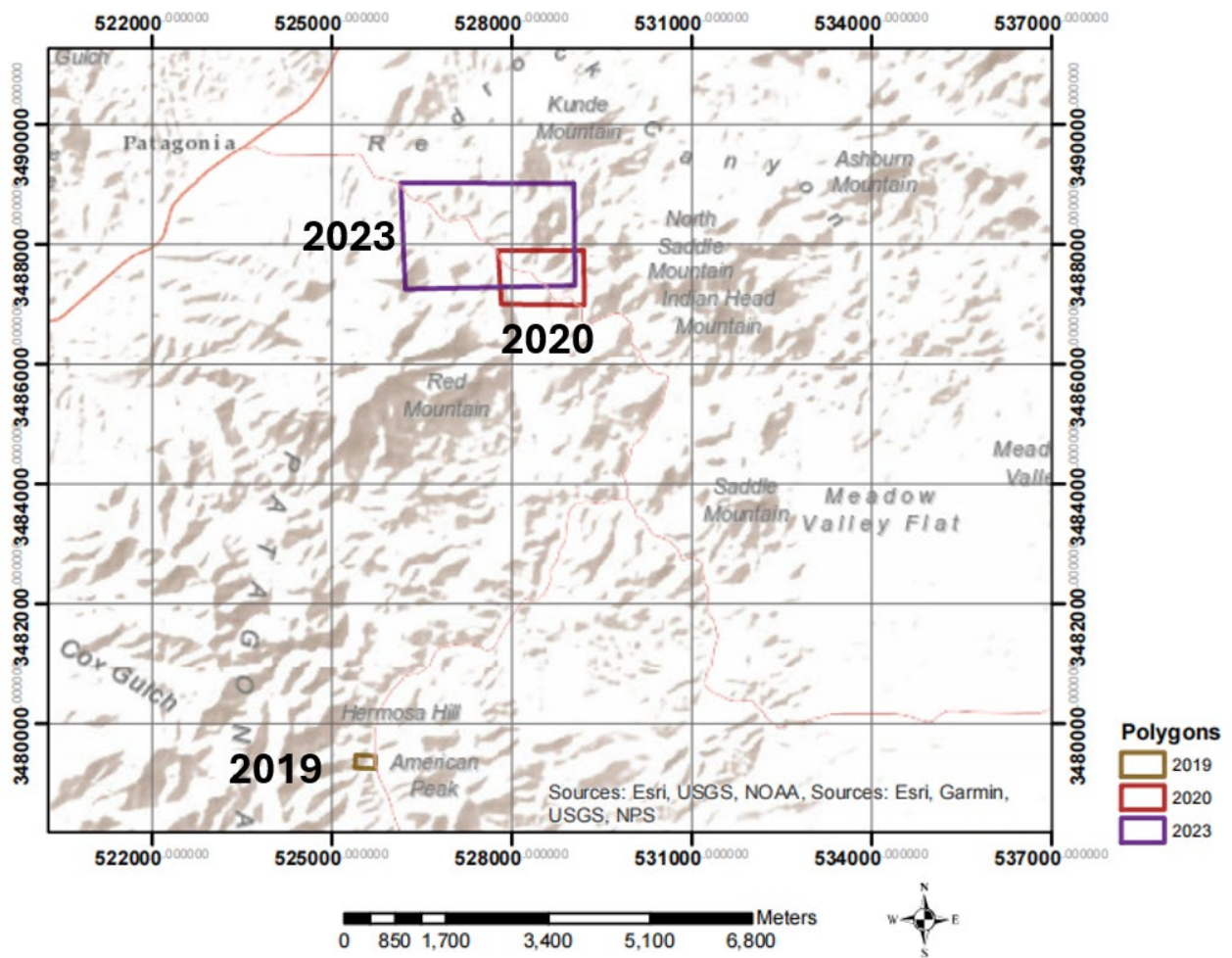


Figure 1.2-3. Geological units of Patagonia Mountain (Simons, 1972; Vikre et al., 2014).

## Geophysical Surveys in the Harshaw Creek Area 2024

The GEOS 416 class from the University of Arizona, under the guidance of the USGS, has performed geophysical surveys in the Patagonia area for many years. Figure 1.2-4 illustrates the areas where surveys were carried out between 2019 and 2023, providing valuable data for comparison with the results obtained this year.



*Figure 1.2-4. Areas where previous surveys were conducted.*

### 1.3 Project History

The SE region of Arizona, characterized by the Santa Rita and Patagonia Mountains, boasts a geological landscape abundant in valuable metal deposits, which has historically fueled extensive mining activities. Recent years have witnessed a surge in mineral exploration and development across the area, driven by favorable metals prices and the accessibility of federal lands for

mining ventures. However, alongside this economic activity, concerns have arisen among stakeholders regarding its potential environmental impacts (Marlow, 2007).

Today, attention is focused on understanding and addressing the ongoing environmental degradation, particularly in areas like the Harshaw Creek watershed. The identification of pollution sources is a crucial first step in evaluating the necessity of reclamation efforts, as water flowing through these areas inevitably encounters exposed minerals, potentially leading to downstream acidification (Dean, 1982).

To solve this issue, the United States Geological Survey (USGS) conducts scientific research aimed at understanding the environmental impacts of mining activities in the area. This research focuses on assessing the release of contaminants into water and soil, providing valuable insights into the extent and severity of contamination, and locating possible water sources. Recent investigations have revealed variations in groundwater quality, particularly on the Red Rock Ranch property. Despite the stream water within Harshaw Creek and the surrounding ranch properties testing within healthy limits, well water on the Red Rock Ranch has shown dangerously high metal concentrations and a low pH. To further understand these variations, geophysical surveys spanning property boundaries have been proposed. These surveys investigate the physical properties of subsurface layers and interpret the lithologic structure and its spatial variation.

Collaborating annually with students from the University of Arizona's GEN 416 class, the USGS conducts geophysical surveys and mapping projects in the area. This year's surveys utilized the direct-current (DC) resistivity method to map subsurface resistivity variations, locate groundwater resources, and characterize their extent, depth, and potential yield. These collaborative efforts contribute to ongoing research and monitoring initiatives to address environmental challenges in the Patagonia Mountains and Harshaw Creek area.

## **1.4 Geologic Background**

### **1.4.1 Geology**

The Patagonia Mountains are located in Santa Cruz County, in SE Arizona. The region has an extensive history of mining, continuing through to today. The Hermosa Mine, owned by South32, is developing the Zn-Pb-Ag Taylor sulfide deposit and the Zn-Mn-Ag Clark oxide deposit (South32, 2024). The basement rocks of the Patagonia mountains, formed in the Proterozoic Eon, are granitic and overlaid by sedimentary and volcanic rocks from the Paleozoic Era. The Harshaw Creek area, where the geophysical data for this study were collected, consists of upper Cretaceous volcanic rocks, including trachyandesite and rhyolite. The surface geology in parts of the study area is Tertiary-Quaternary Basin Fill deposits (Vikre et al., 2014).

The Patagonia Mountains also have an important tectonic history that tells how the rocks formed and deformed in Southern Arizona. During the subduction of the Farallon plate under the North American plate, the North American Cordillera was a contractional system. Once the Farallon plate was fully subducted, the system became extensional and formed the San Andreas Fault. Southern Arizona is still in Basin and Range extension today and the Patagonia Mountains area experiences a combination of normal and thrust faulting (DeCelles et al., 2009).

### **1.4.2 Hydrology**

Flowing NW, Harshaw Creek is a tributary of the Santa Cruz River watershed and lies within the Sonoita Creek Basin. Rainfall during the monsoon season from July through September and snowmelt from nearby high topography in the winter contribute to the streamflow of the creek. Porous rock layers, such as gravel and sand in alluvial deposits store groundwater. Water is also contained in the fractures and faults of the volcanic and metamorphic rocks (Alizadeh-Ahlavi, et. al., 2023).

## **1.5 Sites Description**

Our DC resistivity surveys were utilized in the Lower Harshaw Creek area to identify potential fault structures within the geological framework of SE Santa Rita and N Patagonia Mountains. Three survey lines—PB, PC, and PD—were established to systematically investigate subsurface

resistivity variations indicative of fault presence. We also included an interpretation of last year's resistivity line with Line PC, taken along the road in the same area of the fault (Figure 1.5-1). The locations were based on accessibility and permission from landowners. The final locations represented several different area types along the fault system. The first two parallel lines—PB and PC—are 280 and 275 m in length respectively (Figure 1.5-2). These lines taken along the Patagonia Fault represent several types of structural settings: (1) Line PB: a mountain ridge section; (2) Line PRRC 3 from 2023: a valley edge; (3) Line PC: a valley or central subbasin; (4) Line PD: a complex fault segment into a major Sonoita valley.

Line PD is situated approximately 1.68 km SW of lines PC and PB (Figure 1.5-3). The coordinates of all lines were recorded using the Universal Transverse Mercator (UTM) system, as detailed in Table 1.

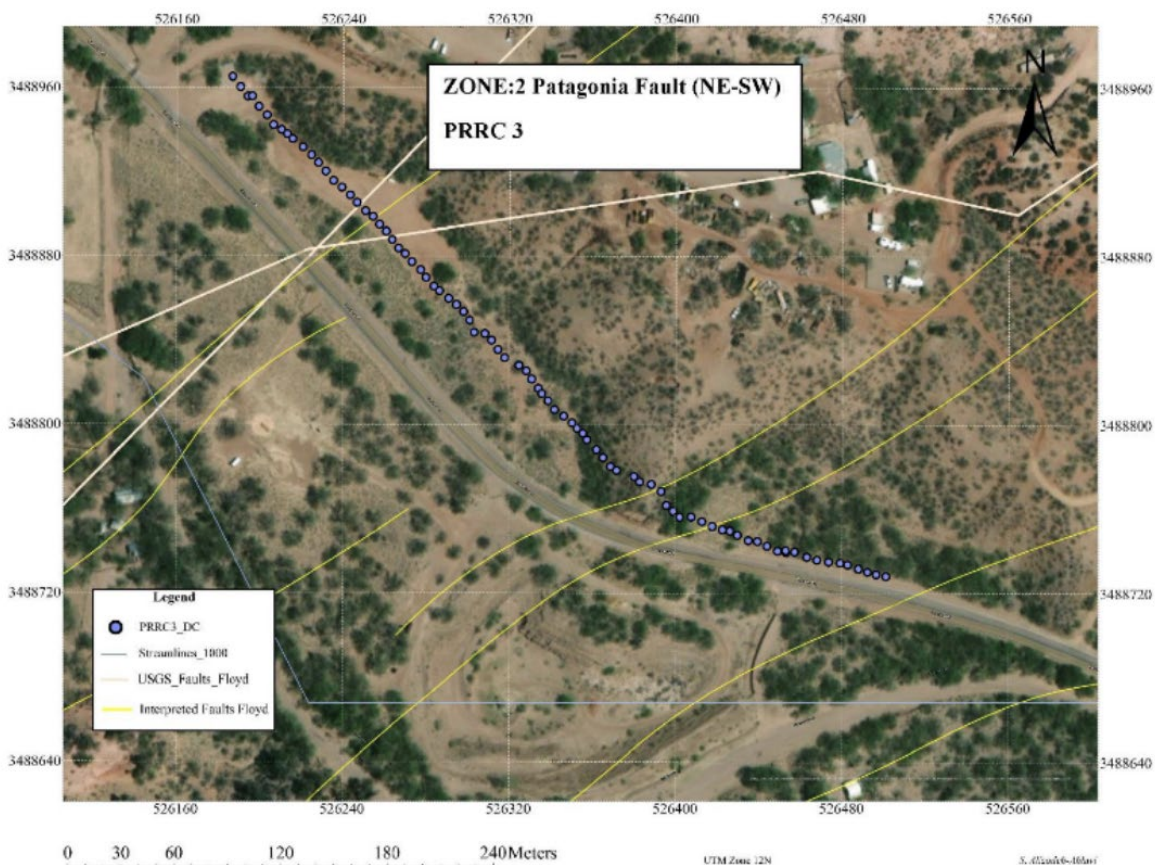


*Figure 1.5-1. Map view of Line PRRC 3 (Geophysical Surveys, 2023).*

Geophysical Surveys in the Harshaw Creek Area 2024



*Figure 1.5-2. Location map of the PB & PC lines. overlaid by the Elgin, AZ, 1932 map.*



*Figure 1.5-3. Location map of the PD Line. overlaid by the Elgin, AZ, 1932 map.*

Geophysical Surveys in the Harshaw Creek Area 2024

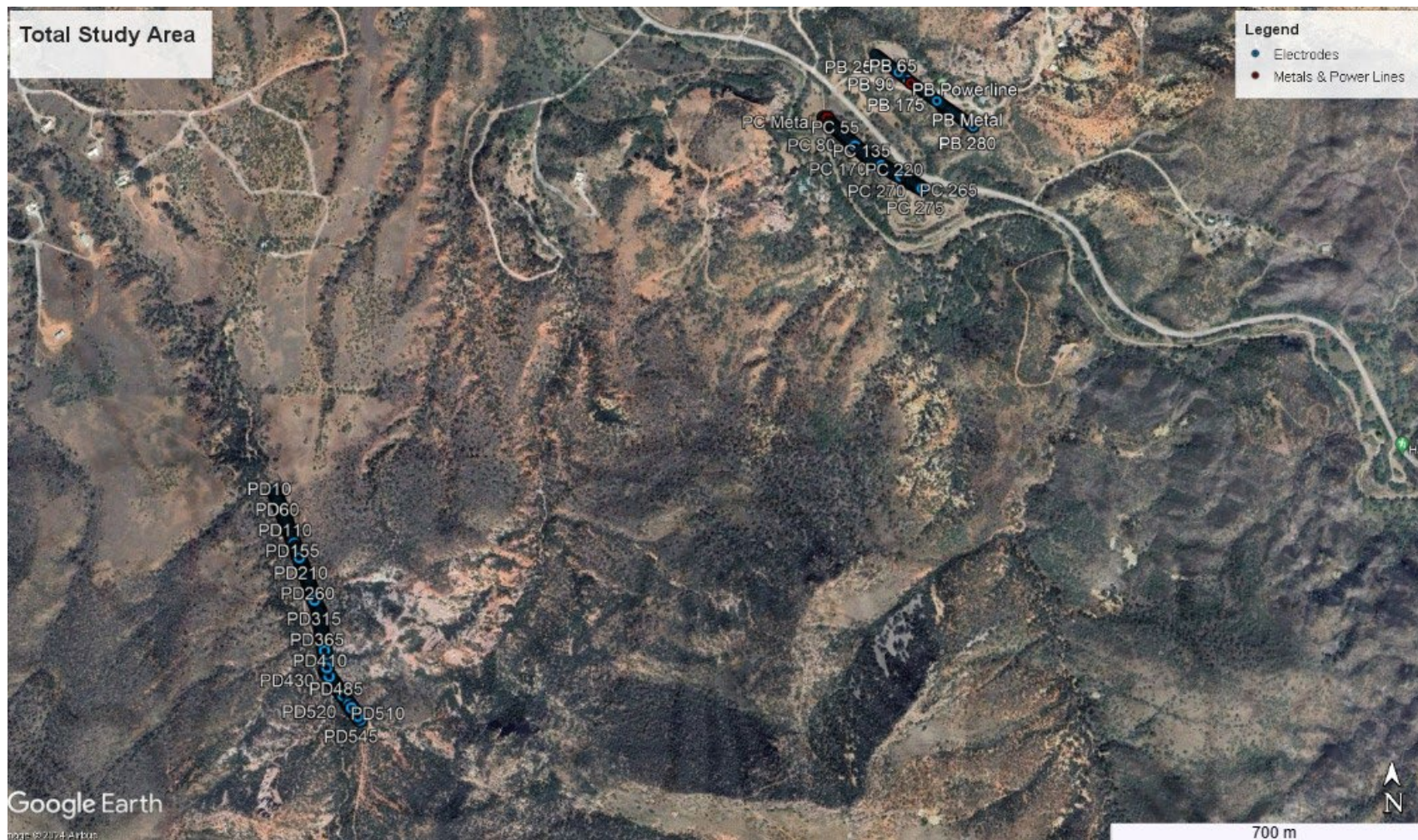


*Figure 1.5-4. Location map of the total study area, overlaid by the Elgin, AZ, 1932 map.*

	Date of Collection	GPS Starting Point	GPS Ending Point
Line PB	February 10, 2024	31.53589899, -110.723564	31.53446702, -110.721337
Line PC	March 3, 2024	31.53468202, -110.724754	31.53323103, -110.722451
Line PD	March 2, 2024	31.52710302, -110.737504	31.52259104, -110.735455

*Table 1.5-1. GPS starting and ending points for each line in UTM coordinates.*

## 2 Methods

### 2.1 Equipment and In-Field Setup

Direct-current resistivity surveys are a nonintrusive geophysical technique that determines the resistivity in the subsurface. Lithologies have various resistivities and thus, with these data, we can locate potential aquifers which will have a low resistivity. Specifically, our surveys used surface dipole-dipole and strong gradient electrode arrays containing 56 electrodes at 5 m spacing. Figure 2.1-2 explains how each electrode connects to the other 55 electrodes to produce apparent resistivity data points of the subsurface (seen in red in Figure 2.1-1). Electrodes 0–27 are called the “source” nodes, which send current through the ground and to the “sink” electrodes 28–56. Resistivity is collected at each resistivity data point by calculating the voltage potential difference between every two nodes, following Ohm’s Law:

$$R = \frac{V}{I}$$

*Equation 2.1-1. Ohm’s Law*

showing the relation between resistivity (R), voltage (V), and current (I). By varying the spacing between electrodes, the resolution and depth of collection can change. For instance, less space

between electrodes will lead to higher resolution since the subsurface data points will be closer together. Our 5 m spacing allows high-resolution resistivity data up to ~60 m depths.

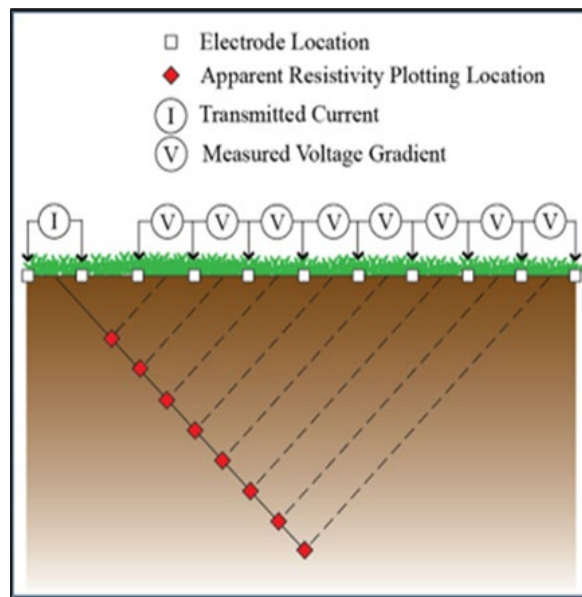


*Figure 2.1-1. Dipole-dipole schematic showing subsurface resistivity data collection (EPA, 2016).*

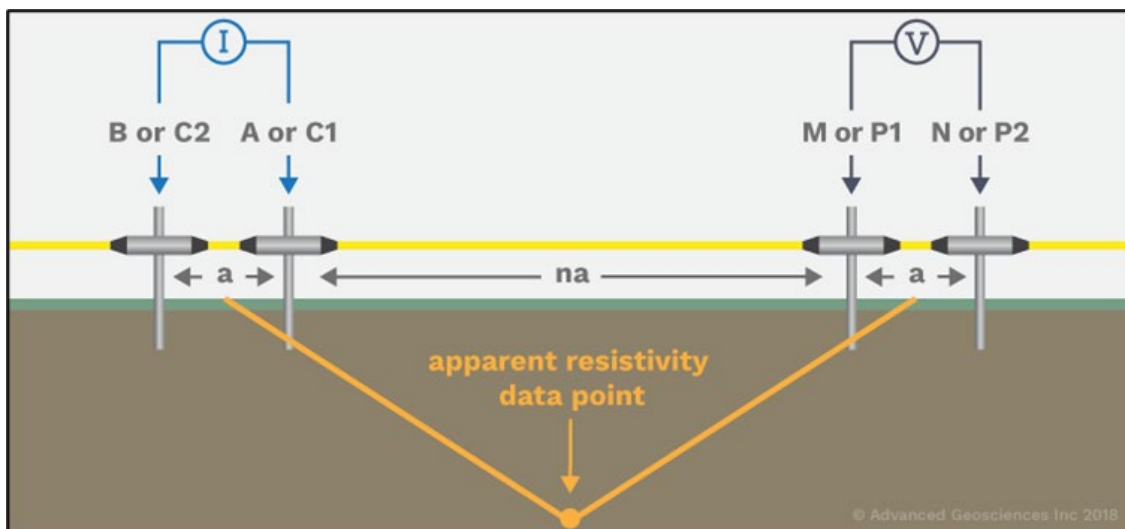


*Figure 2.1-2. Dipole-dipole schematic showing data collection in more detail (EPA, 2016).*

Figure 2.1-3 shows the setup of an electrode. Each electrode is coupled to the ground by a spring and stake. Small divots were carved and filled with salt water to ensure connectivity with the subsurface. To provide current and voltage to electrodes, we used AGI SuperSting R8 connected to a 2kW generator attached to AC/DC power (Figure 2.1-4). A resistivity test was run

before each survey to ensure proper connectivity. During data collection, the AGI SuperSting R8 automatically collects two resistivity values at each subsurface point. The two values must be within 2% of each other, otherwise the machine repeats the data collection at the subsurface point.



*Figure 2.1-3. Electrode array setups. Figure 2.1-4. AGI SuperSting R8 connected to a 2kW generator.*

The surveys included two 275 m lines (Lines PB and PC) and a 555 m line (Line PD) SW of Patagonia, projected to contain the Patagonia Fault. The 555 m line was created through a “roll-along” technique. These data were collected on February 10, March 3, and March 2, 2024, respectively. For all lines, GPS coordinates and elevation were marked every 70 m using the Garmin GPSMAP® 64st, and intermediate locations were interpolated. If present, GPS coordinates were also recorded for power lines, metal pieces, and fences along the array to correlate with potential errors in pseudosections.

## **2.2 Data Processing Using AGI EarthImager 2D**

To process the data collected from the resistivity lines, we used the AGI EarthImager 2D software through the USGS license. The pseudosections in this study were generated using this software. The data for one of the resistivity lines is first loaded onto a computer with the software installed and then into the program. A pseudosection of the measured apparent resistivity is generated. Next, we ran a smooth model inversion on the data. This process

generates a pseudosection of the calculated apparent resistivity below the measured pseudosection and the inverted resistivity pseudosection at the bottom. To generate the inverted pseudosection, a model is fit to the data and refit until the model converges. Each inversion for our resistivity lines stopped at the fifth iteration. A root mean squared error or RMS between the predicted and measured data is calculated to measure goodness of fit. We aimed for RMS values below 5% for the pseudosections.

$$RMS = \sqrt{\frac{\sum_{i=1}^N \left( \frac{d_i^{Pred} - d_i^{Meas}}{d_i^{Meas}} \right)^2}{N}} \cdot 100\%$$

**Equation 2.2-1. Root Mean Squared Error**

N is the total number of data points,  $d_i^{Pred}$  are the predicted values of the data points,  $d_i^{Meas}$  are the measured values of the data points, and  $i$  represents each point as the summation iterates from 1 to N. If the model produced too high of an RMS, we removed noisy data and performed another inversion. We utilized a data misfit scatter plot to visualize areas and points where the most error occurred. Areas in between and around the points were interpolated by the model to generate a smooth visualization of the resistivity. Pseudosections for each line were generated independently. After each inversion was generated, GPS data collected from the field containing elevation, latitude, and longitude were added. This shows the elevation profile of each line. For the test line, 339 of 1756 (19.27%) measurements were removed and there was an RMS of 4.82%. No data were removed from Lines PB and PC and an RMS of 4.11% and 3.79% were achieved respectively. Each of these lines has 1756 measurements. For Line PD, 408 of the 4186 (9.75%) measurements were removed and an RMS of 5.44% was achieved. Since all of the lines were either geographically far from each other or on different geological layers, the upper bound of the color scales for each line differs. The bottom bound is set at 20 Ohm-m for each line.

It should be noted that the calculated and measured sections are similar but contrast the inverted section, which exhibits more prominent structural features. The inverted section is not assumed to be overinterpreted because the software corrects for lower resolution at depth due to diminishing electrical flow.

## 2.3 Archie's Equation

Archie's equation is relevant to our investigation of subsurface structures and hydrogeology due to its widely applicable explanation of rock and water resistivities. This empirical equation relates measured resistivities to porosity and saturation in the following equation:

$$\rho = a\varphi^{-m}S_w^{-n}\rho_w$$

*Equation 2.3-1. Archie's Law*

where  $\rho$  is measured rock resistivity,  $\varphi$  is fractional porosity,  $s_w$  is fractional volume water saturation, and  $\rho_w$  is the effective pore water resistivity. The constants  $a$ ,  $m$ , and  $n$  are typically  $0.5 \leq a \leq 2.5$ ,  $1.3 \leq m \leq 2.5$ , and  $n \approx 2$  (Reynolds et al., 1997). Constants  $a$ , the tortuosity exponent, and  $m$ , the cementation factor value, are determined from the logarithmic plot of the formation factor ( $F$ ) and porosity ( $\varphi$ ), where  $F$  is  $\frac{\rho}{\rho_w}$ . Constant  $n$ , the saturation exponent value, is determined from the log-log plot of the resistivity index ( $I_r$ ) and fractional porosity ( $s_w$ ) (Mohamad et al., 2017).

Electrical resistivity measures the resistance of the flow of electric current within a geomaterial. When considering the geometric factor, such as the electrode array, we get apparent resistivity ( $\rho_a$ ), which then has units of Ohm-m. The reciprocal of electrical resistance is electrical conductivity ( $\sigma$ ), which has units of  $S\ m^{-1}$  (Choo et al., 2014).

Interpreting our pseudosections with respect to Archie's equation, lower resistivities and higher conductivities are a result of higher porosity and water saturation. Higher resistivity corresponds to lower water concentrations.

## 2.4 Test Site

On our first day in the field, we performed a test survey aiming to acquaint ourselves with the equipment and methodologies essential for our surveys in the Harshaw Creek of the Patagonia mountains. Utilizing direct current resistivity (DCR) equipment provided by the USGS, we arranged 56 electrodes in a linear configuration to ensure thorough coverage of our target area. Each electrode was positioned at 5 m intervals and connected to a 2kW generator via a spring attachment. After collecting data, USGS member Jamie Macy provided invaluable guidance on

interpreting the data, generating inverted pseudosection using the AGI EarthImager 2D, and understanding the subsurface resistivity variations along the traverse using the pseudosection.

This first resistivity survey we conducted was in a wash between two streets in a residential neighborhood in Casas Adobes, Arizona. This line is referred to as the Line 6702 or the test line. Due to possibly unsafe weather conditions in Patagonia, Arizona on Saturday, February 10, 2024, we determined that a test survey would be useful for us to become familiar with the equipment and process. The line runs N to S between two streets, N Casas Adobes Dr and N Calle Lomita. The line began at 32.328883, -110.969911 and ended at 32.326422, -110.969989. This survey crossed several private property lines as shown in Figure 2.4-1. We obtained permission from each property owner.

Figure 2.4-2 shows the pseudosection we generated for this survey. The blue color represents low resistivity, green indicates medium, and red signifies a high-resistivity layer. There is a clear boundary between the resistive and conductive layers, situated approximately 10 m deep. Water concentration peaks between 10–34 m depth. The surface layer exhibits the highest resistivity, ranging from 340–857 Ohm-m.

After completing this test survey, we gained a deeper understanding of DC resistivity data interpretation and its relevance in hydrological analysis and approached our subsequent surveys with confidence.

Geophysical Surveys in the Harshaw Creek Area 2024



Figure 2.4-1. Location map of the 6702 test line.

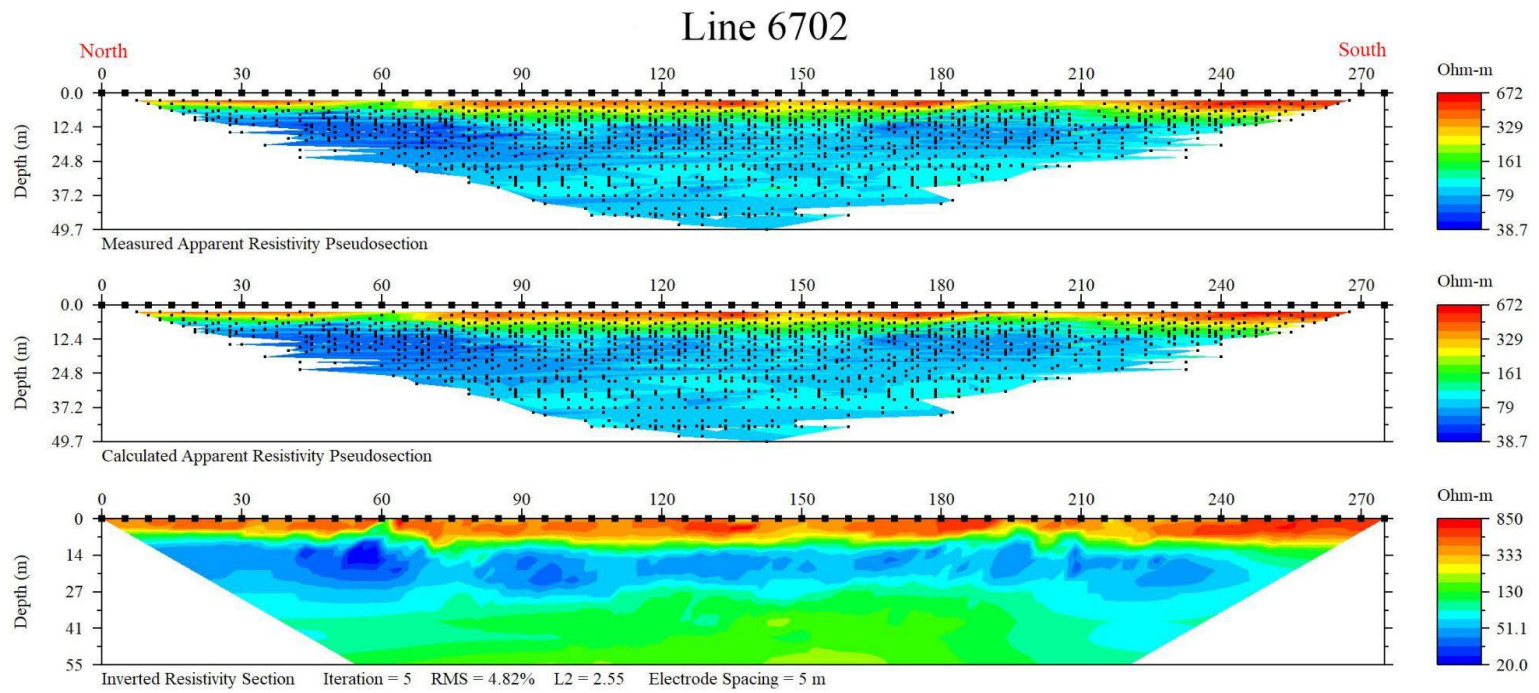


*Figure 2.4-2. DC resistivity results, showing the subsurface properties of Line 6702.*

## 3 Results and Interpretations

### General Assumptions

Regarding the interpretation of the pseudosections, general assumptions must be made about how basin and range faulting affects preferential water flow and how subsurface structures manifest in surface features. Down dropped bedrock blocks (horsts) associated with basin and range faulting accommodate sediment fill in basins (grabens). These basins are deepest adjacent to the multiple subparallel complex faults. Alluvium infill is composed of highly connected porous sediments with considerable water-holding capacity. In our pseudosections, low resistivity is associated with alluvium. Broken bedrock, however, has little water-holding capacity. High resistivity is associated with bedrock. On the surface, these discrete fault zones are manifested in highlands and lowlands. Shearing destroys rock surrounding the fault, forming a lowland of finer material. Unsheared rock outcrops on either side of the fault. It is assumed, therefore, that the fault lies in the lowland between highlands within the fault zone. Another notable surface manifestation of a fault includes tree lines. Sheared rock is weaker than bedrock, establishing a pathway for water, facilitating tree growth. Rock outcrops are more reliable than tree lines since they are less variable in formation. Comparing surface features to geophysical data produces the most reliable interpretations. The topographical features allow us to project the fault zones through precise electrode locations in our lines, corresponding to subsurface features shown in our pseudosections.

The DC resistivity results shed light on the subsurface properties, including the rock types, which allow us to infer any geologic structures based on the displacement of rock bodies. The possible rock types corresponding to the resistivity (in Ohm-m) are shown in Figure 3.0-1. For resistivities between 1 and 1000 Ohm-m, common materials are sedimentary rocks, weathered igneous rocks, and fresh water. The unweathered igneous and metamorphic rocks have a resistivity greater than 1000 Ohm-m, i.e. low conductivity.

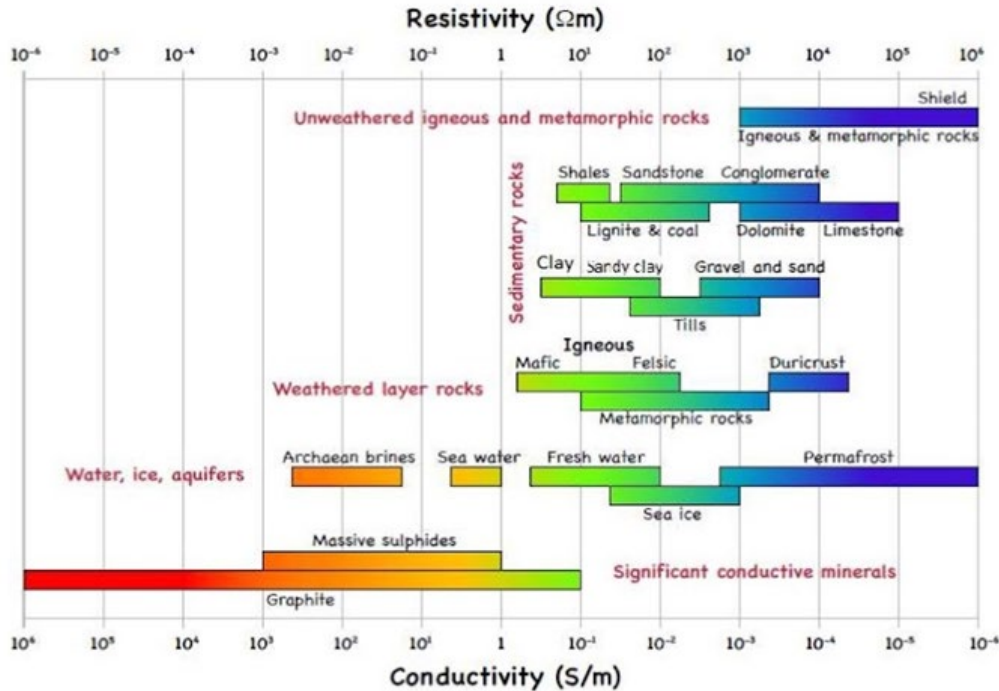


**Figure 3.0-1.** Resistivity and conductivity for various rock types  
(Miensofust 2010; Palacky 1987; Marti 2006).

### 3.1 Line PB

Line PB is surveyed on Dave Martin’s property, located of the Town of Patagonia. The line starts at 31.53589899, -110.723564 and ends at 31.53446702, -110.721337, with a total length of 275 m (Figure 3.1-1). The surface is covered with consolidated sediments from the beginning to loose soil starting at station 200. There is minimal elevation change along the line. In addition, the line is situated at a mountain ridge (Figure 3.1-2).

The potential fault lines are identified by features such as lineament, tree lines, and shear zones formed between two outstanding rock outcrops shown in the aerial photo. Their intersections with Line PB are determined after extending the potential fault lines to the area of Line PB by assuming that the traces of faults are perfectly straight (Figure 3.1-3). Four fault lines have been identified, which intersect with the survey line at stations 25, 120, 150, and 205. These intersections are seen in the zoomed-out map. The aerial indication of the first and third fault lines (from left to right) is a lineament that commonly forms in the fault zones; the indicator for the

## Geophysical Surveys in the Harshaw Creek Area 2024

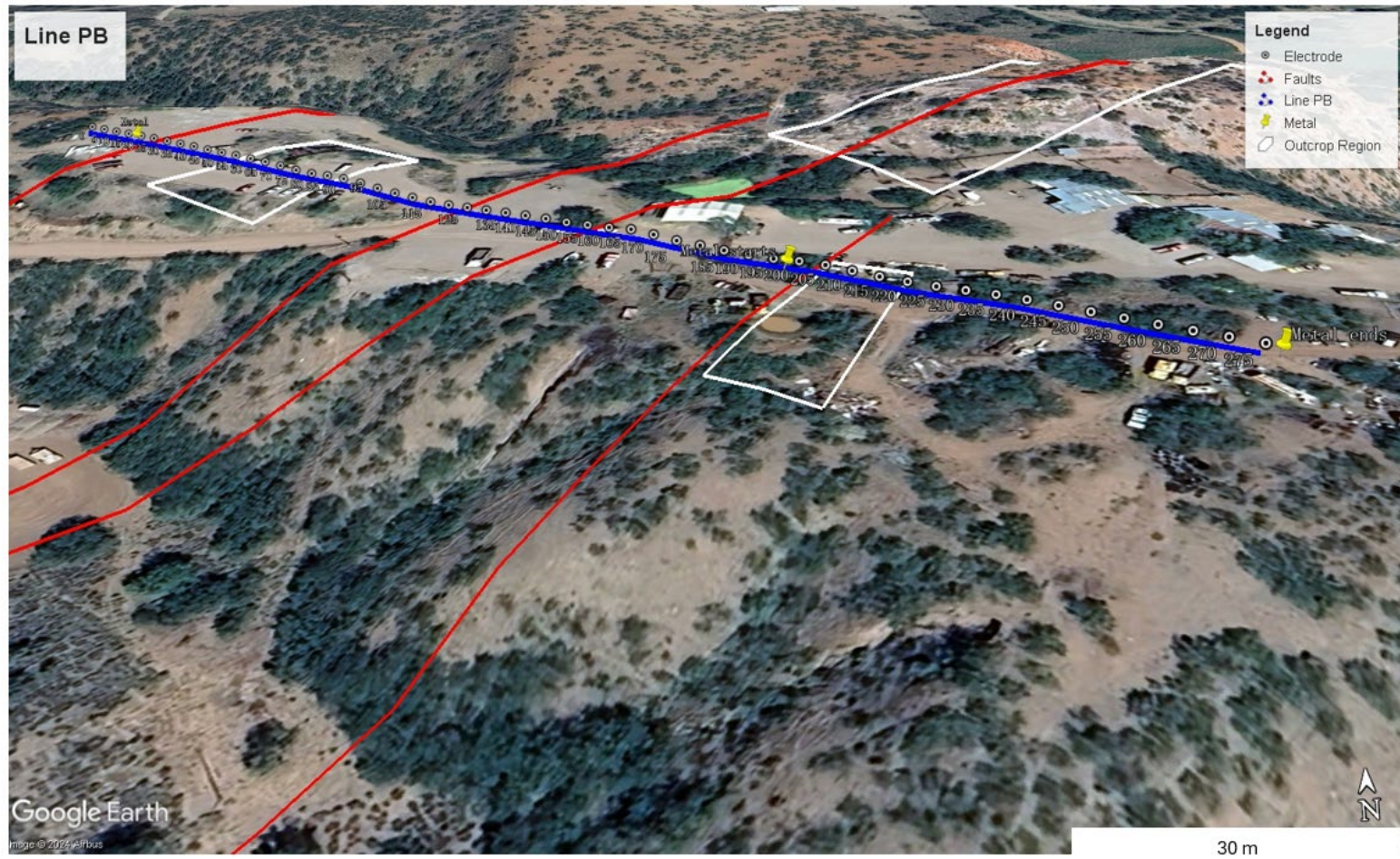
second and fourth fault lines is a tree line, which is less credible compared to exposed rock structures but still provides useful information as they were also identified in the class report of 2023.

# Geophysical Surveys in the Harshaw Creek Area 2024

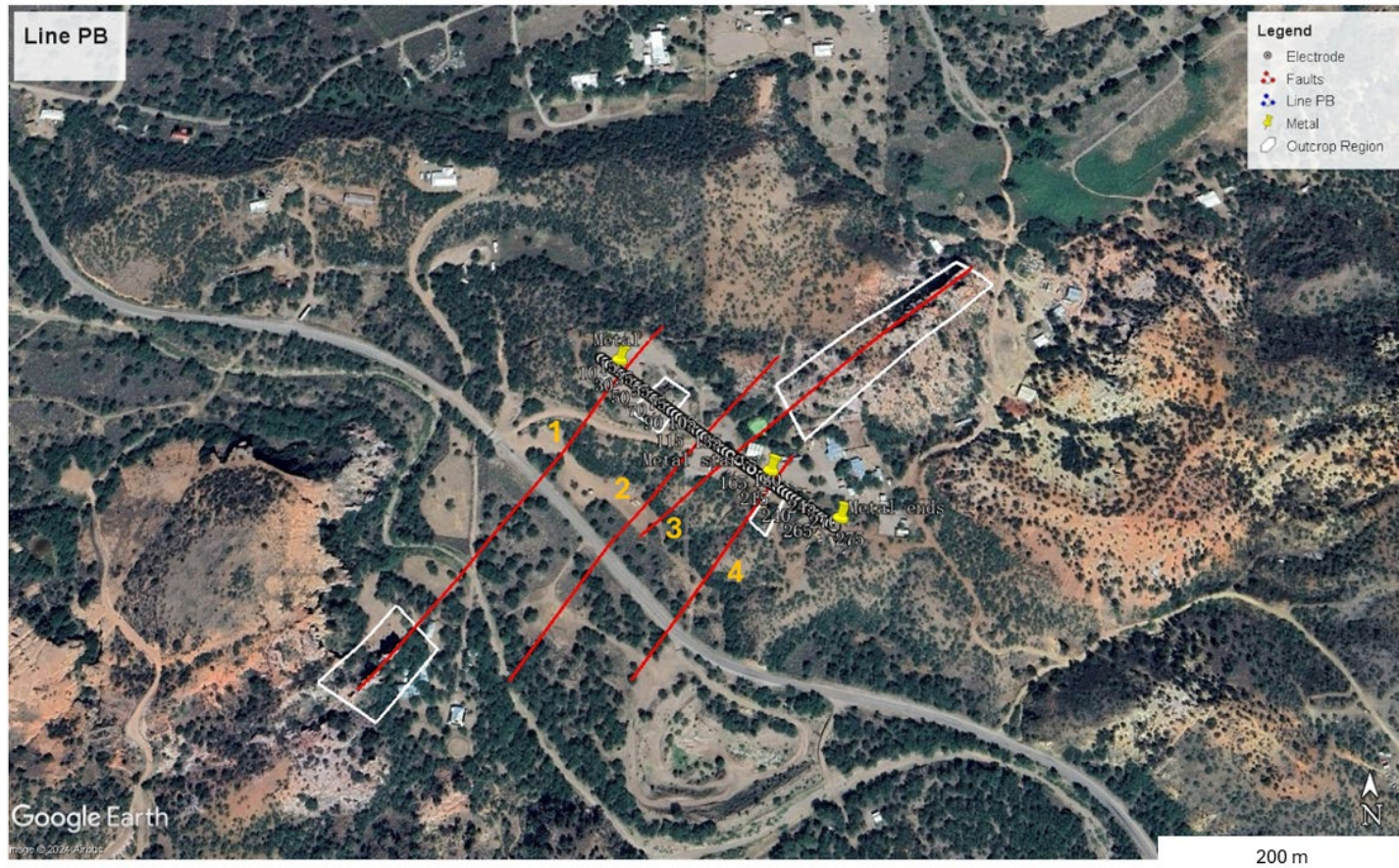


Figure 3.1-1. Map of the Line PB with potential fault lines.

# Geophysical Surveys in the Harshaw Creek Area 2024



*Figure 3.1-2. Map of Line PB with potential fault lines shown with elevation.*



*Figure 3.1-3. Map of the entire region, which shows the potential traced fault lines and their intersections with Line PB.*

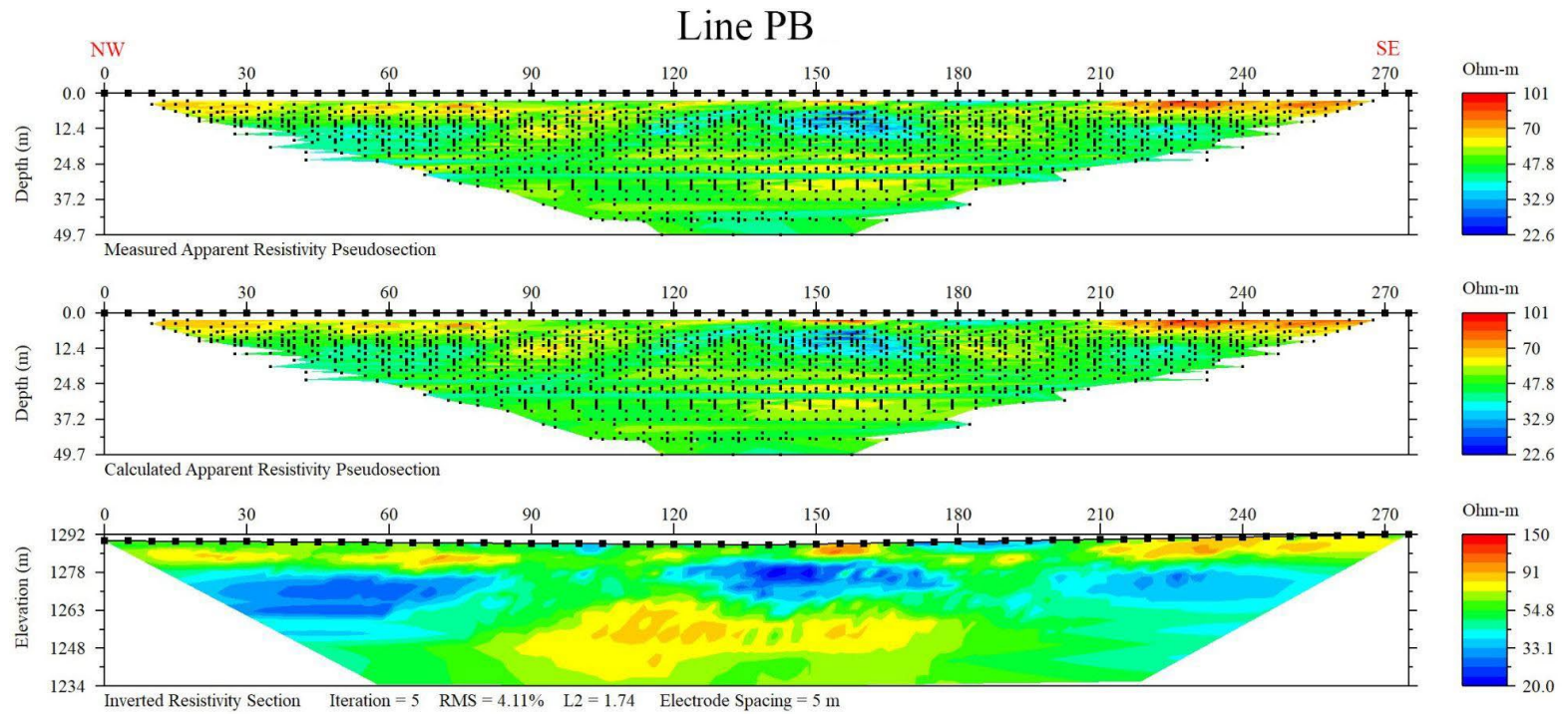


*Figure 3.1-4. DC resistivity results showing the subsurface properties for Line PB.*

Figure 3.1-4 shows the DC resistivity results for Line PB. The cross-section after the inversion (bottom panel) has a subsurface resistivity ranging from ~20–150 Ohm-m, indicating the materials that compose the subsurface can be fresh water, sedimentary rocks, and weathered igneous and metamorphic rocks. Based on the field observations, the majority of materials that reside in the shallow surface are sandy clay, which is consistent with the resistivity data showing a background subsurface resistivity of ~55 Ohm-m. The highest resistivity is observed between stations 150 and 170 at the surface. The lowest resistivity is found in a pattern of discrete blocks suited to the middle layer at 14–44 m depth.

The prominent features indicated by the DC resistivity test are three low-resistivity bodies situated at ~15–45 m depth. These relatively conductive layers appear from stations 15–80, 120–180, and 200–250. Based on the hypothesis that there are regional faults present, these low-resistivity bodies are interpreted as water pockets that formed due to secondary porosities in the permeable sandy clay layers. In addition, the water pockets provide clues on the location of the faults. Together with the evidence of the elevated and exposed outcrops, the boundaries of the subsurface faults are determined to be situated at stations 90 and 210. Overall, available data support the existence of subbasins, which are small-scale drawdowns that happen due to the displacement of adjacent rock blocks that contribute to creating conduits for seepage to happen.

Figure 3.1-5 shows the combined aerial image and the pseudosection. Although the potential faults indicated by surface features do not clearly show up in the pseudosection, they are consistent with the location of water pockets, which are produced by fractures (Figure 3.3-5).

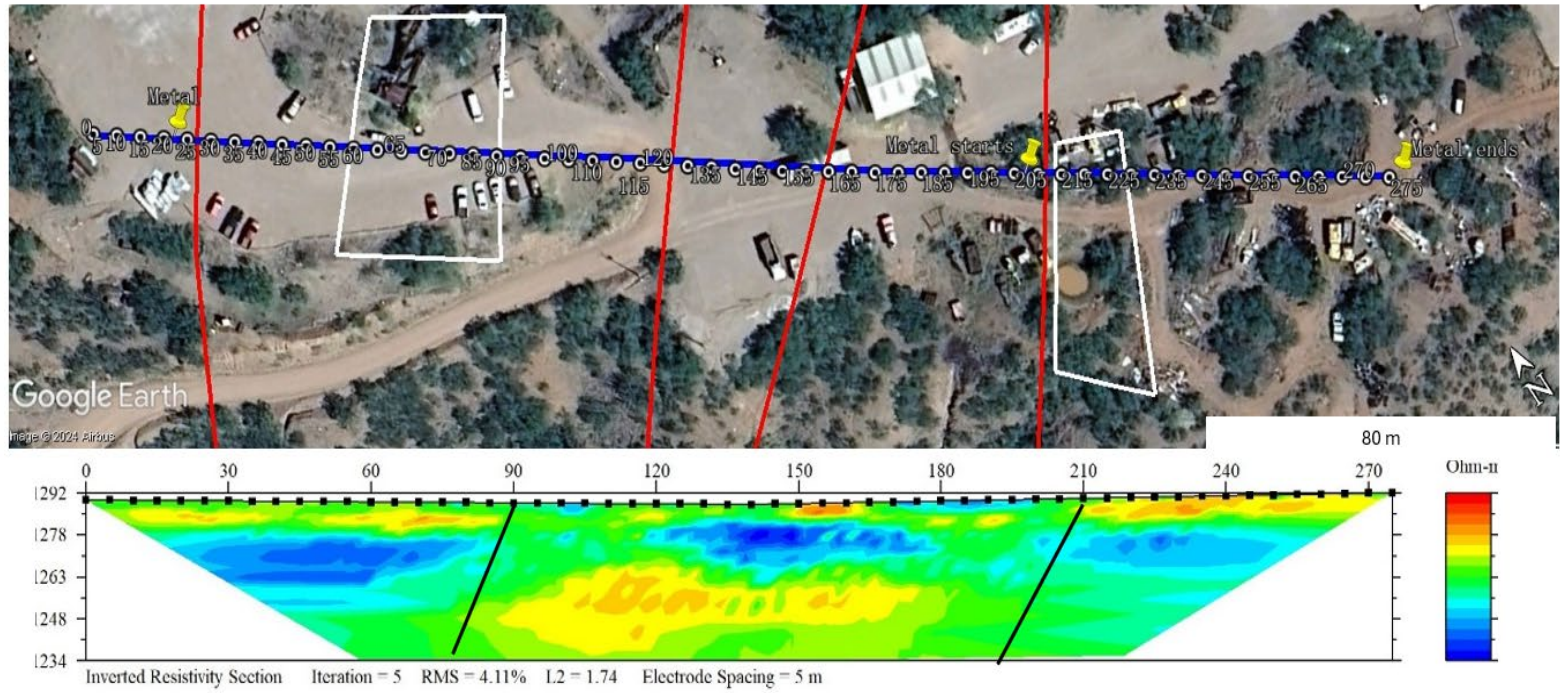


*Figure 3.1-5. Pseudosection with the PB line.*

### 3.2 Line PC

From the DC resistivity data collected from Line PC, the area is interpreted as having multiple complex subparallel faults with similar orientations derived from faulting. To better understand the subsurface location and orientation of these fault zones, aerial features are projected onto Line PC, where the closest electrode they intersect can identify locations of corresponding subsurface features. Four linear features were found and projected onto Line PC (Figure 3.2-2). These aerial linear features included vegetated lowlands between outcrops, where shear zones occur, and ridges perpendicular to the line. Figure 3.2-3 show how the surface aerial projections compare with our subsurface apparent resistivity data at the same locations.

The linear ridge intersects the line at station 75. This area on our apparent resistivity pseudosection shows a break between a resistive layer at ~15 m depth. The resistive red layer is interpreted as sandy clay, due to the location of our line in a valley. The lowland features intersect the line at stations 140 and 240, where breaks between resistive layers are also seen at around 15 m depth. The areas where the resistive layer (sandy clay) is offset are interpreted as shear zones and act as pathways for water. Station 140 sits above a relatively low resistivity material and in between offset resistive layers. Overall, four fault zones offsetting sandy clay at ~15 m depth are interpreted from the DC resistivity data. Sitting at the bottom of the pseudosection is a conductive, unbroken layer at 20 Ohm-m. This is interpreted as water-rich sandstone, where station 140 possibly acts as a pathway from the surface to the water table.

Figure 3.2-4 shows how Line PC runs through a valley with resistive, higher relief topography to the NE and SW of the line. Since water pools in valleys that sit between high topography, water can form in pockets of porous rock, like the sandstone at 35–52 m depth in the apparent resistivity pseudosection.

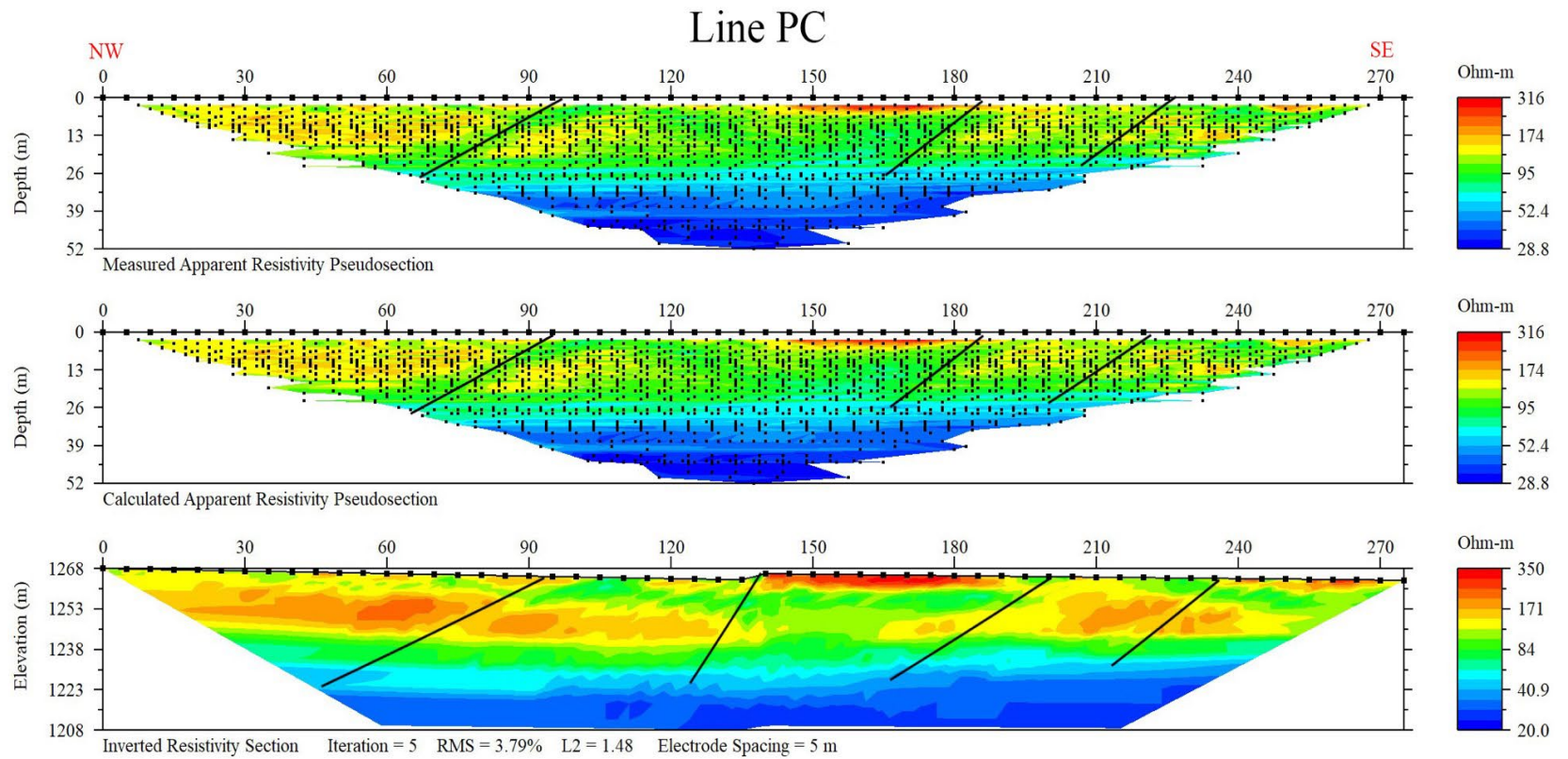


*Figure 3.2-1. Results of the DC resistivity measurements for Line PC, showing where breaks occur in a layer on the calculated, inverted, and apparent resistivity pseudosections.*

Geophysical Surveys in the Harshaw Creek Area 2024



*Figure 3.2-2. Aerial image of the area around Line PC showing the linear features identified and projected onto the line.*

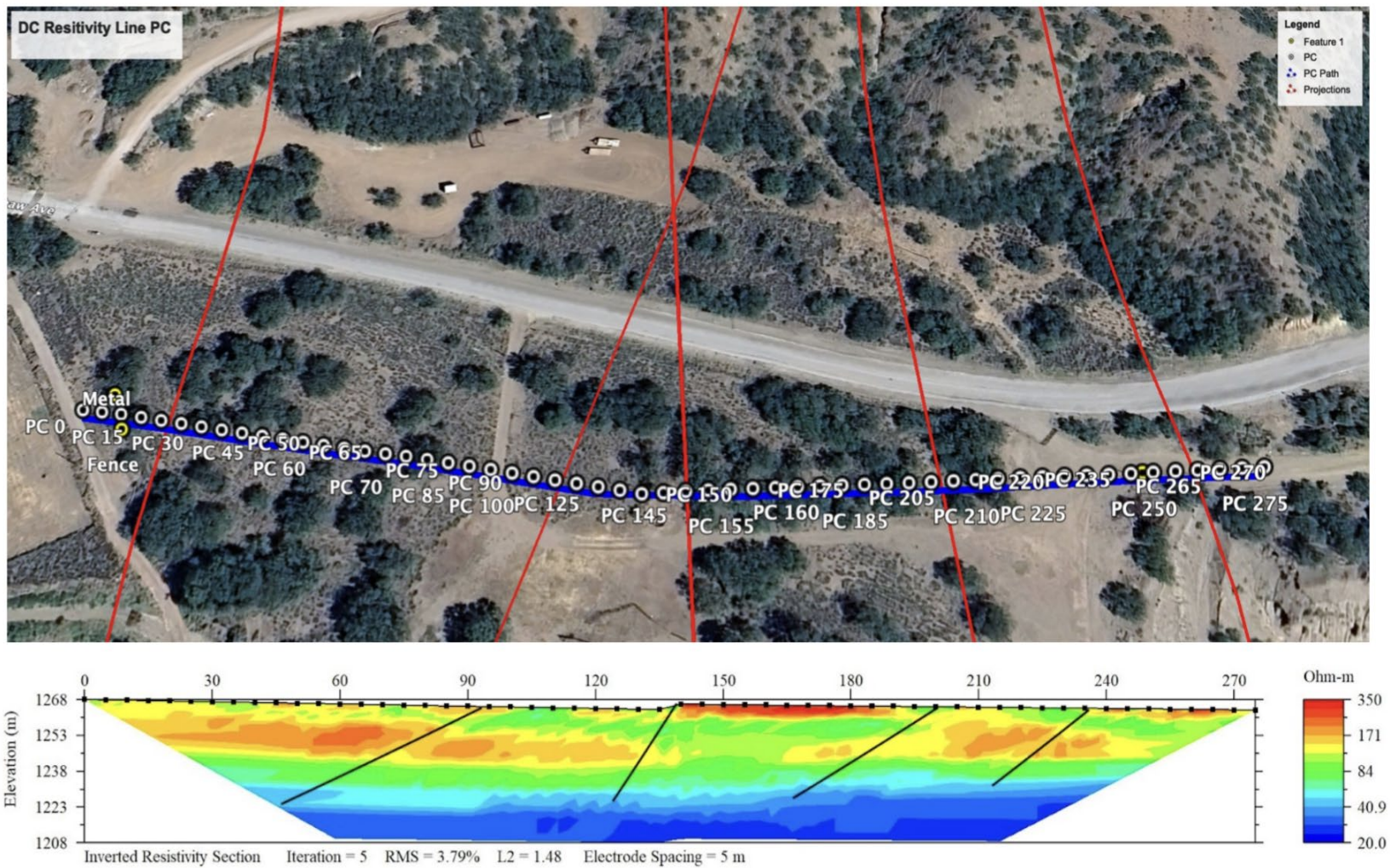


*Figure 3.2-3. Projected linear features assembled with the apparent resistivity pseudosection, showing where features seen on the surface are similar to subsurface features.*

# Geophysical Surveys in the Harshaw Creek Area 2024

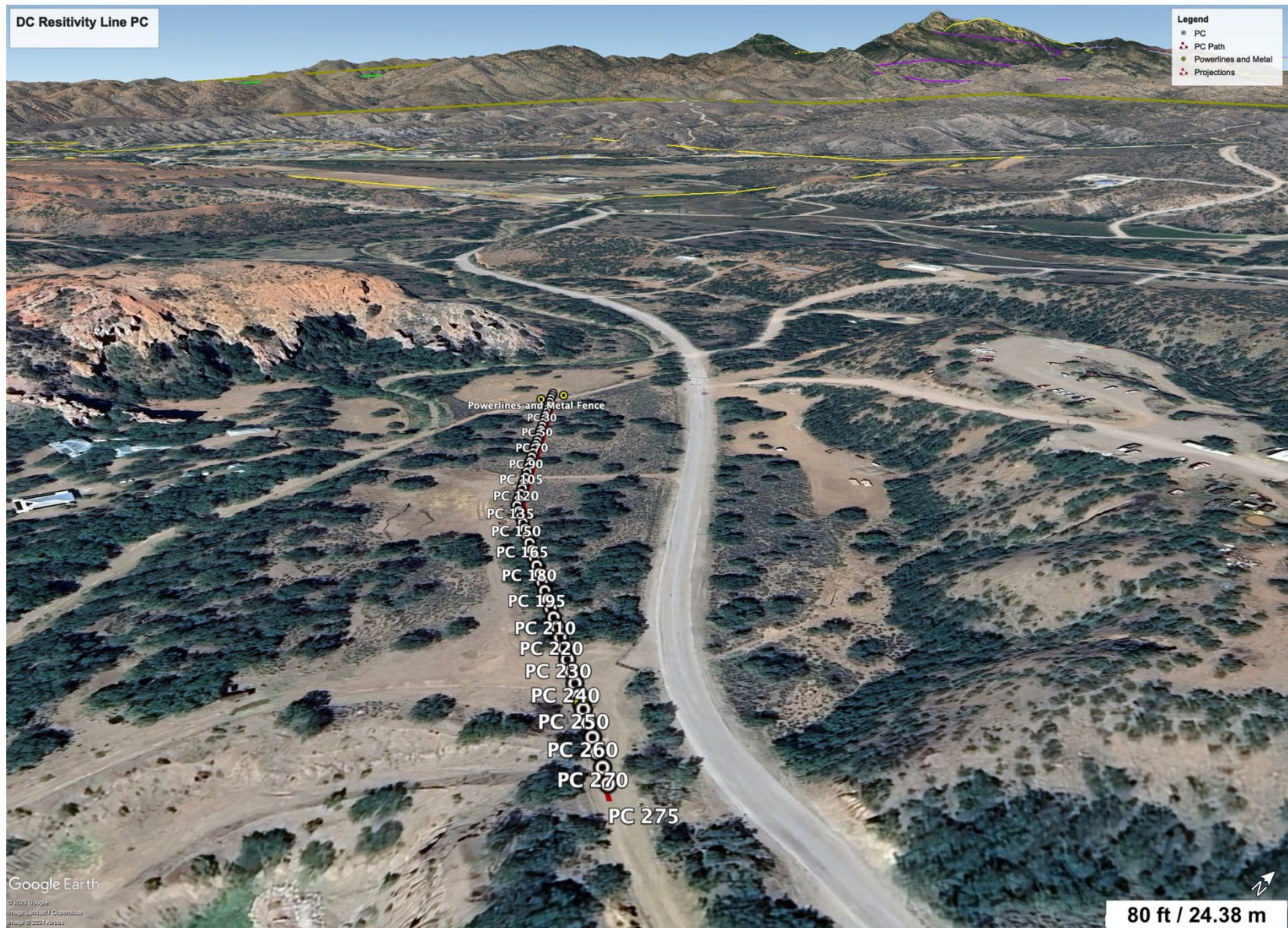


*Figure 3.2-4. 3-dimensional aerial view contrasting the topographical relief between Line PC and the surrounding mountains.*

### 3.3 Line PD

As seen in section 1.5, Line PD lies in the National Forest Service boundary, SE of Patagonia and SW of Lines PB and PC. Line PD starts at 31.52710302, -110.737504 and ends at 31.52259104, -110.735455. After two “roll-alongs,” the total length of the line is 555 m (Figure 1.5-4). The last third of the line is primarily running down a forest service road.

As described in *General Assumptions*, Southern Arizona is characterized as a basin and range province. Line PD lies on a clean edge of a fault that dropped into the main valley. Surrounding topography can be seen in Figure 3.3-1. Here, we see the S end of the line terminates at the onset of a 100–130 m wide valley at the base of Red Mountain. The N end of the line terminates toward the town of Patagonia to the NW, which is a natural alluvial basin. Line PD lies between two smaller mountains. Surrounding topography translates to larger elevation differences between stations compared to other surveys. Compared to the Vikre et al. (2014) geology map (Figure 3.3-2), Line PD cuts perpendicular to the approximate location of the Patagonia Fault at station 315. However, our geophysical data show that the complexity of the fault zone extends beyond one single fault line. Our fault zone cuts unconsolidated quaternary gravel deposits (QTg) to the NW and Red Mountain volcanics (TKr) to the SE. Cretaceous andesite (Ka) is also present in the valley just S of our line.

From an aerial perspective (Figure 3.3-3), three separate tree lines projected through stations 540, 485, and 315 run along topographical lowlands (yellow). In the pseudosection (Figure 3.3-4), station 540 overlies a basin beyond the depth of investigation; station 485 overlies a shallower basin; and station 315 overlies a pocket of porous material. Two separate rock outcrops projecting through stations 420 and 280 run along topographical highlands (white) and coincide with pronounced topographical corrections in the pseudosection. Regarding the 420 outcrop, the electrodes corresponding to stations 415 and 420 were hammered directly into bedrock in the field, unlike all other electrodes which were hammered into alluvium. Additionally, from stations 420 to 445, a highly resistive lithology protrudes through the surface. Our first interpreted fault, F1, (red) follows another tree line along a lowland adjacent to the 420 rock outcrop. F1 is projected through station 395. F2 (dashed line) projects through station 345 and is inferred primarily from a laterally terminating, resistive lithology in the pseudosection.

Although ambiguous at the surface, F2 is drawn along a contact between a red-brown and gray rock unit seen in the map view. Similar to F1, F3 follows a tree line along a lowland adjacent to the 280 rock outcrop. F3 is projected through station 250. The final interpreted fault, F4, follows a faint tree line but is apparent in the pseudosection, similar to F2, running along a terminating, resistive lithology.

Stations 445 to 555 in the pseudosection are within a conductive region of  $\sim 20$ – $1,000$  Ohm-m, partially extending beyond the depth of investigation. The resistivity increases slightly below  $\sim 39$  m depth. We interpret this as a sediment valley filled with a sandstone/sandy-clay lithology. This sediment has potential for holding water, owing to connected porosity. This conductive region likely extends SE into the broad valley. This relatively water-rich region and organic layer likely explain why the first 8 m from the surface is relatively conductive at  $\sim 20$ – $120$  Ohm-m.

The region between stations 360–445, overlying the most prominent feature in the pseudosection, contains a highly resistive NW-dipping layer of  $\sim 10,000$  Ohm-m. This layer was seen protruding through the surface at stations 415 and 420. The rock seen in the field was either a rhyolite/andesite bedrock. F1 is inferred to cut through this bedrock extending to depth. F2 is inferred to lie at the termination of this highly resistive layer and the onset of a low resistivity pocket of porous material. We interpret this feature as a down-dropped bedrock block (horst) associated with movement along F1 and F2.

The region between F2 and F3/F4 and stations 250 and 350 is characterized by a lower resistivity lithology of  $\sim 447$  Ohm-m from  $\sim 0$ – $26$  m depth. There is a higher resistivity lithology of  $\sim 2115$  Ohm-m below the low resistive lithology. We interpret the lower resistivity lithology to be a pocket filled with the sandstone/sandy-clay lithology with a potential mixture of conglomerates due to surface observations. The sediment fill is deepest ( $\sim 39$  m) under station 315 where there is a lowland as seen in the aerial view. We interpret the underlying higher resistivity layer to be the same lithology as the prominent, NW-dipping layer: rhyolite/andesite bedrock. The fault zone dropped this horst down in a classic basin and range stepping feature (Figure 3.3-5). To the NW of F3/F4, we infer that there is another down-dropped block.

We predict that just NW of F3/4, there may be another down dropped horst below our depth of investigation (e.g. 300 m deep). In future studies, deeper geophysical surveys will better constrain the depth and water-holding capacity of the basin. It should be noted that all our interpreted faults have a NW-dip. This pseudosection represents a classic slip-fault motion in a basin and range region where the horst closest to the surface dips the deepest (the ~10,000 Ohm-m layer), as this is where the fault movement is the greatest. The subsequent down-stepping layers then flatten out. This fault zone shears surrounding rock, creating a permeable area, as seen by the pocket of porous material between stations 255–335 at ~447 Ohm-m, extending to a depth of 40 m. Forming similarly, other pockets of porous material with the same resistivity are seen throughout the fault zone, extending from F4 to the SE end of the line.

Lastly, from F4 to the NW end of the line is the most conductive zone of the pseudosection with a resistivity ~95–447 Ohm-m. This zone extends to the maximum depth of investigation. Our interpretation is that bedrock from the SE is pushing water to the surface, creating this conductive zone, beginning at the town's alluvial basin.

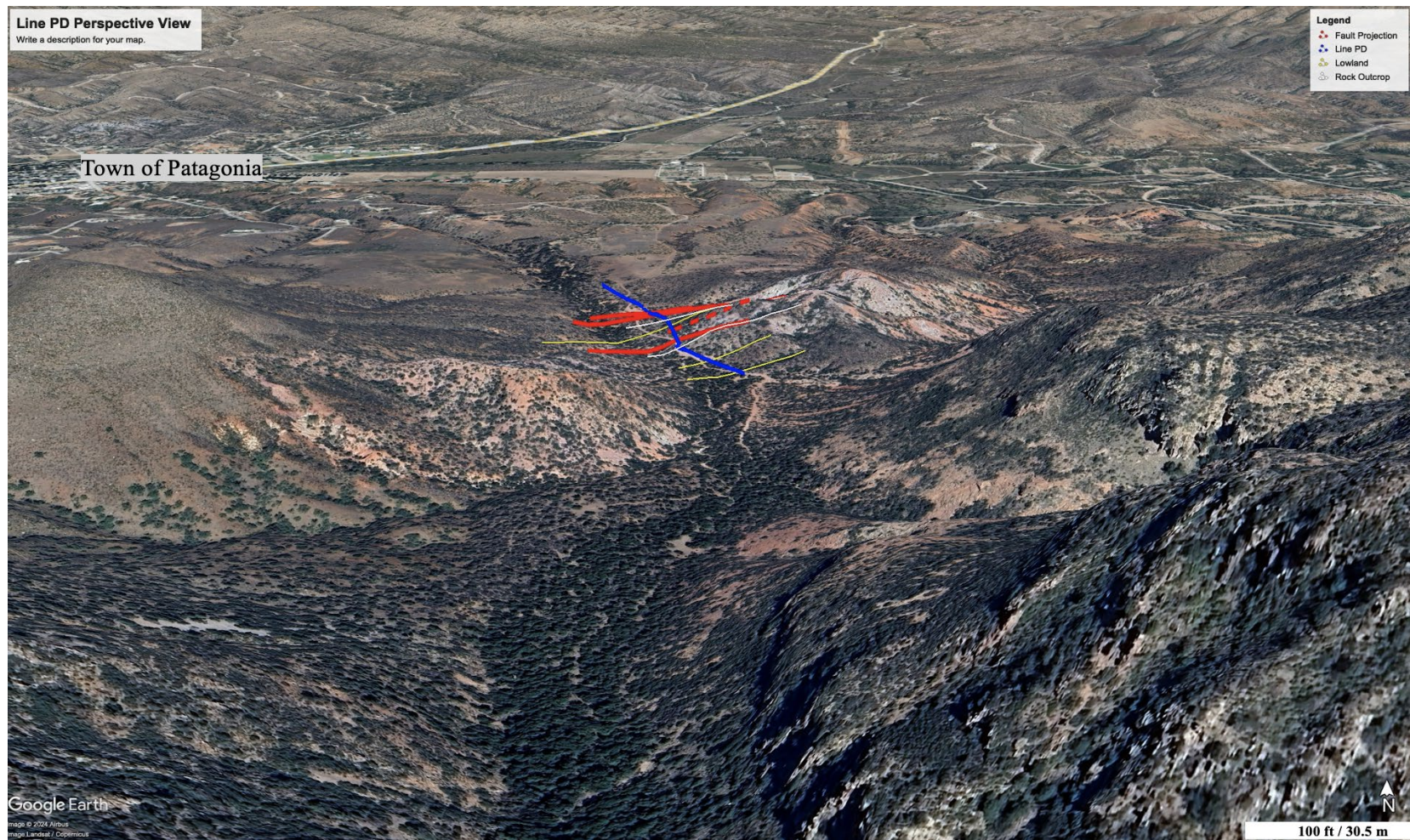


*Figure 3.3-1. The perspective view of Line PD depicts the surrounding landscape, including the 100–130 m wide valley at the S end of the line and the Town of Patagonia.*

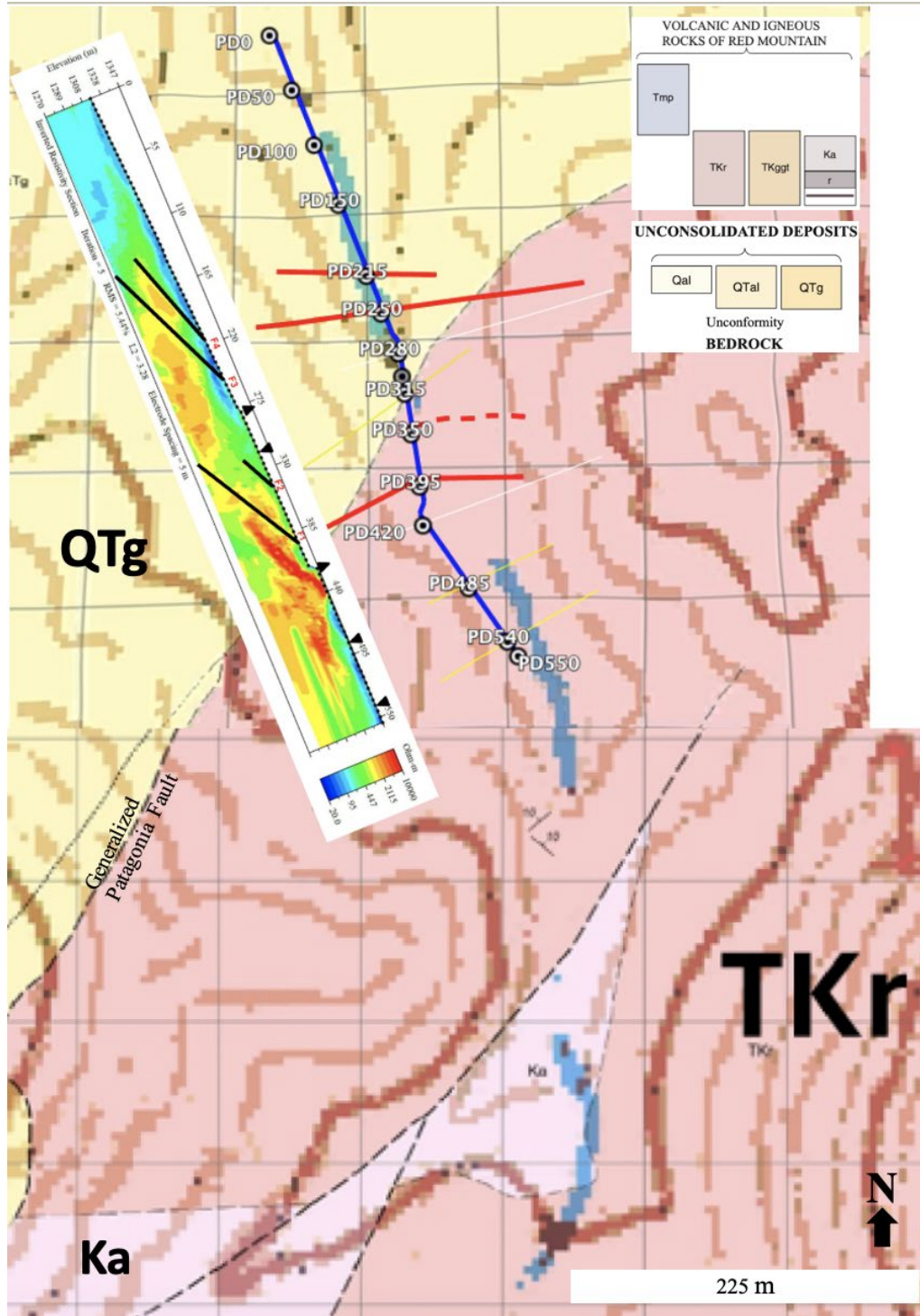


*Figure 3.3-2. Line PD cuts the Patagonia Fault depicted on the Vikre et al. (2014) geologic map. The Line PD pseudosection is overlain on the geologic map to relate geologic and structural surface observations to geophysical data.*

# Geophysical Surveys in the Harshaw Creek Area 2024

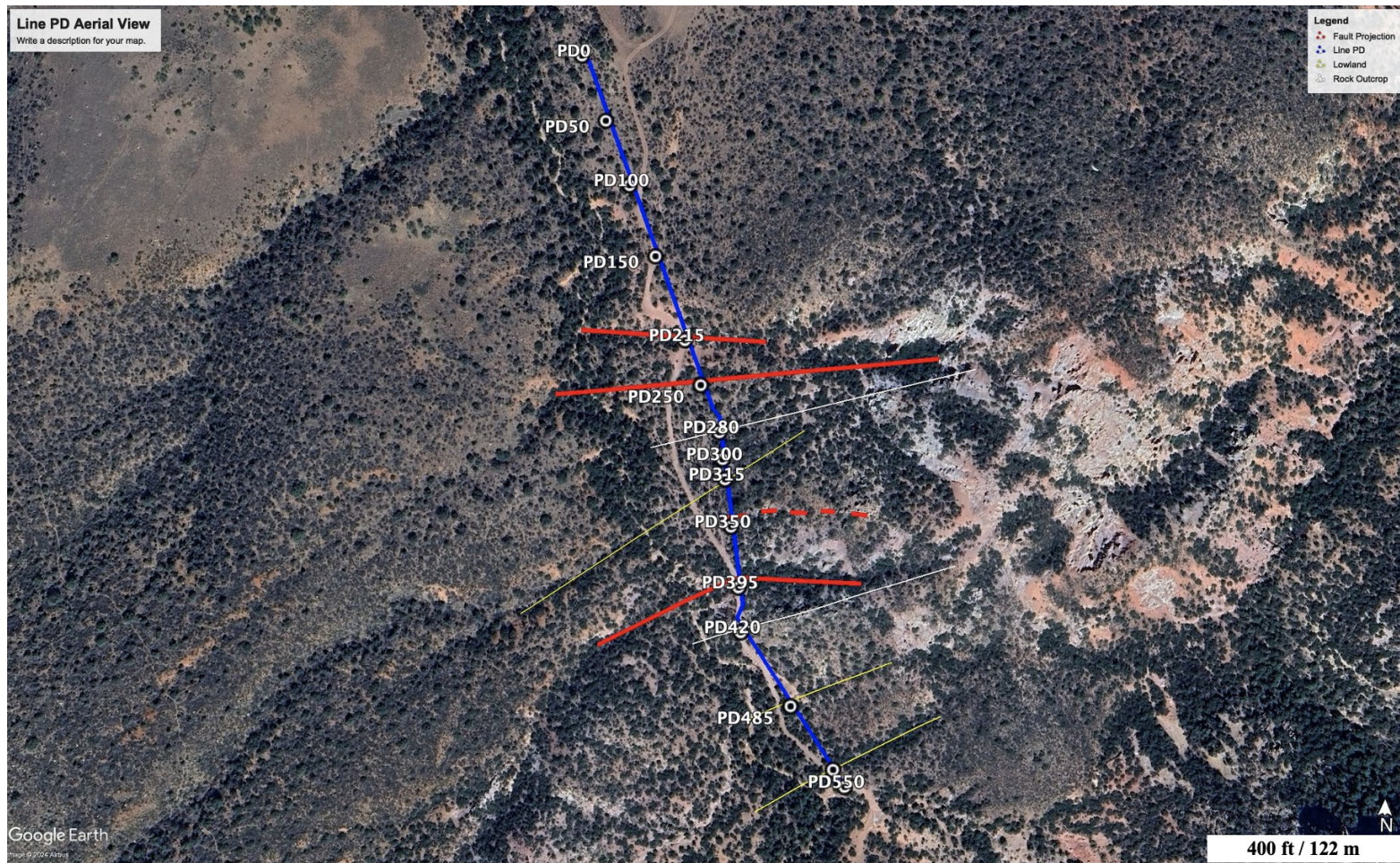


**Figure 3.3-3.** Line PD aerial view with notable features such as faults (red), lowlands (yellow), and highlands/rock outcrops (white).

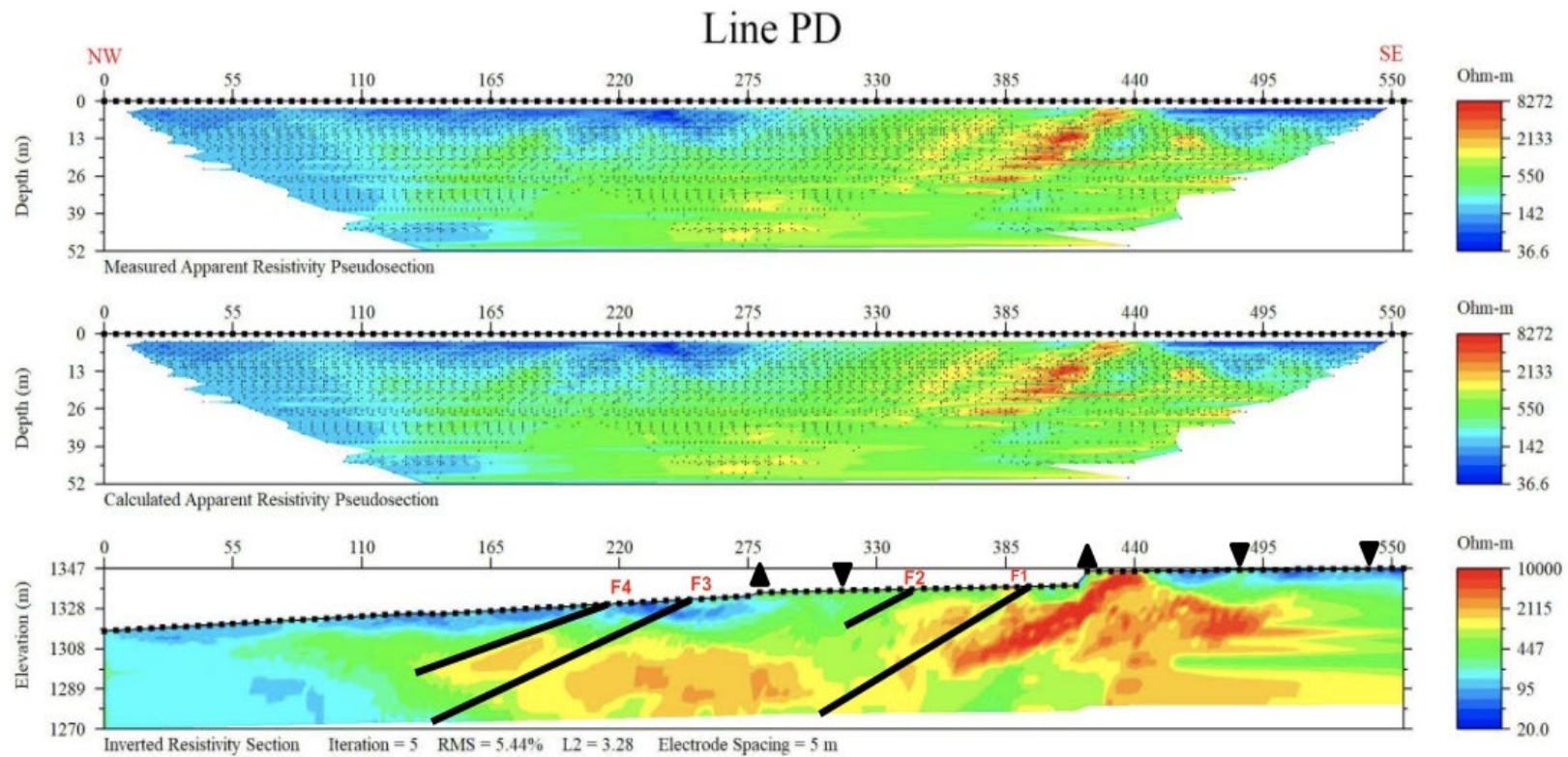


**Figure 3.3-4.** Line PD pseudosection, including projected faults (black lines), lowlands (inverted triangles), and highlands/rock outcrops (upright triangles). Elevation corrections have been applied. The left of the line is to the NW and the right of the line is to the SE.

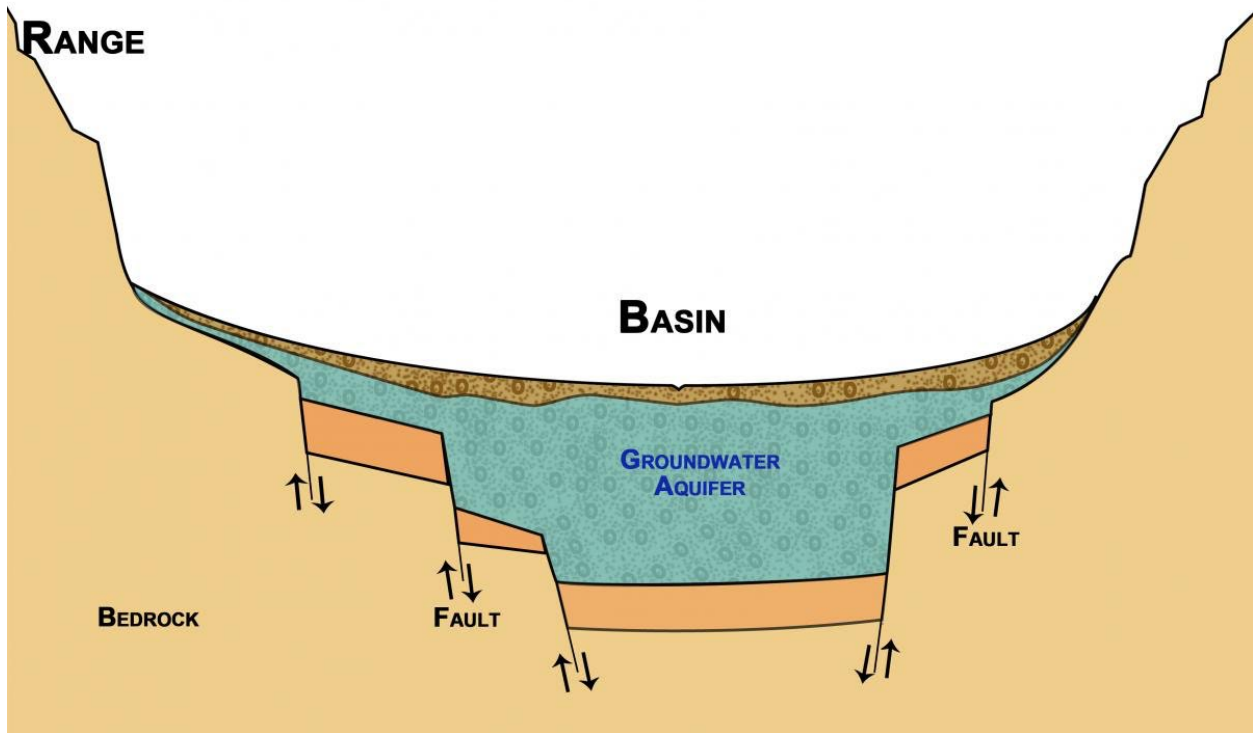


*Figure 3.3-5. Schematic view of Arizona's basin and range province including normal faulting, bedrock horsts and grabens, and groundwater aquifers filled in with unconsolidated sediments (Conway, 2016).*

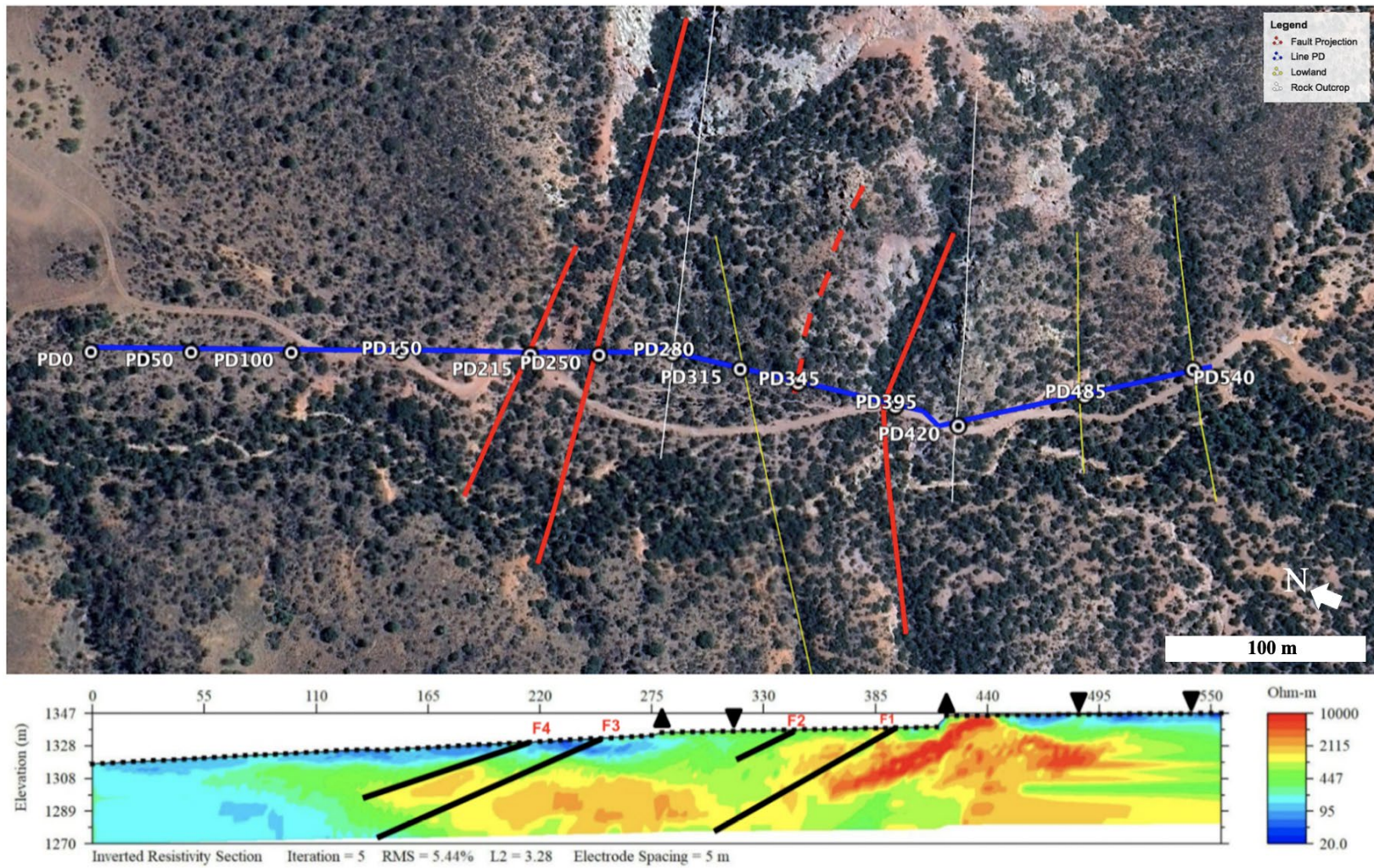


*Figure 3.3-6. Projected surface features coupled with the apparent resistivity pseudosection.*

## 4 Conclusions

Correlating aerial and surface features with our geophysical data provides valuable insight into the structure and water pathways of the Patagonia Fault Zone. The three geophysical surveys correspond to different settings surrounding the fault: a mountain ridge, a valley or central sub basin, and a characteristic basin and range faulting region. Each line produced multiple NW-dipping faults, demonstrating a complex system of faults.

Line PB was located on a mountain ridge NE of the Town of Patagonia and Harshaw Ave. The aerial view projected four potential faults through Line PB. Bedding offset and location of sediment fill narrowed our interpretation down to two faults through stations 90 and 210. The majority of the lithology was a sandy-clay (~54.8 Ohm-m). Three low-resistivity bodies at 15–45 m depth at stations 15–80, 120–180, and 200–250 were interpreted as water pockets—potential aquifers—within the sandy-clay with other smaller sub basins present. Line PC was located in a valley or central sub basin NE of Patagonia but S of Harshaw Ave. The aerial view and pseudosections projected four faults through stations 95, 140, 200, and 235. The fragmented resistive layer (~171 Ohm-m) was a sandy-clay sitting above ~26 m depth. Faulting induces water pathways down to a low-resistivity layer below ~39 m depth, especially under station 140. This layer is interpreted to be the water table. Our final line, Line PD, lies in a characteristic basin and range faulting region SE of Patagonia and SW of Lines PB and PC. Four faults were projected through the line through stations 215, 250, 350, and 395. The faults correspond to two identified horsts of a rhyolitic/andesitic composition (~10,000 Ohm-m). A subsequent inferred horst might be present further into Patagonia’s alluvial basin but exceeds our depth of investigation. The SE and NW low-resistivity portions of our line as well as a smaller pocket between stations 250 and 350 contain sandstone/sandy-clay and potentially conglomerate (~20–1,000 Ohm-m).

Our geophysical results demonstrate complex faulting associated with a basin and range structure. Building from previous works, we can also characterize the depth of the alluvial basin and other micro basins throughout this region. Preferential water flow concurrent with the faults and water holding capacity of porous material may also be better understood surrounding the Patagonia Fault Zone.

## **4.1 Future work**

For the PB line, future investigation is suggested in the northern area in between the current survey line and the outcrops to better characterize the faults. The survey line's depth should be raised to better observe the water table, as the current screen depth is insufficient for visibility. Conducting further DC resistivity or other geophysical surveys in the valley where Line PC is located would be useful in further exploration of the water table as well as for identification of subbasins associated with the Patagonia fault system. For Line PD, we recommend extending the depth of the geophysical survey. This could identify a third, deeper horst and will constrain the depth of potential aquifers or water-bearing porous-material pockets. Overall, drill logs near all lines will identify lithology. Testing water composition, especially in Line PC's water table or areas affected by mining, will aid in identifying water flow and chemical hazards.

## 5 Appendix

### 5.1 Misfit Scatter Plots

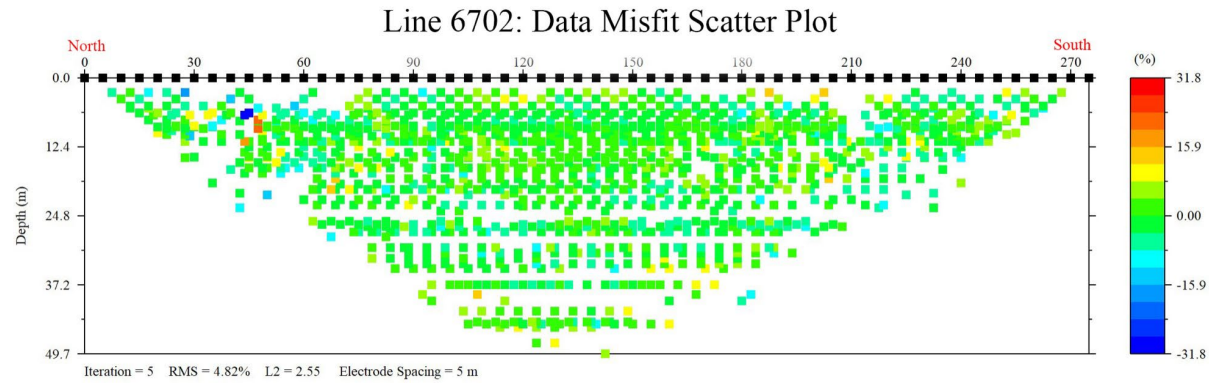


*Figure 5.1-1. The misfit scatter plot measures the error rate between measured and calculated resistivity for Line 6702.*

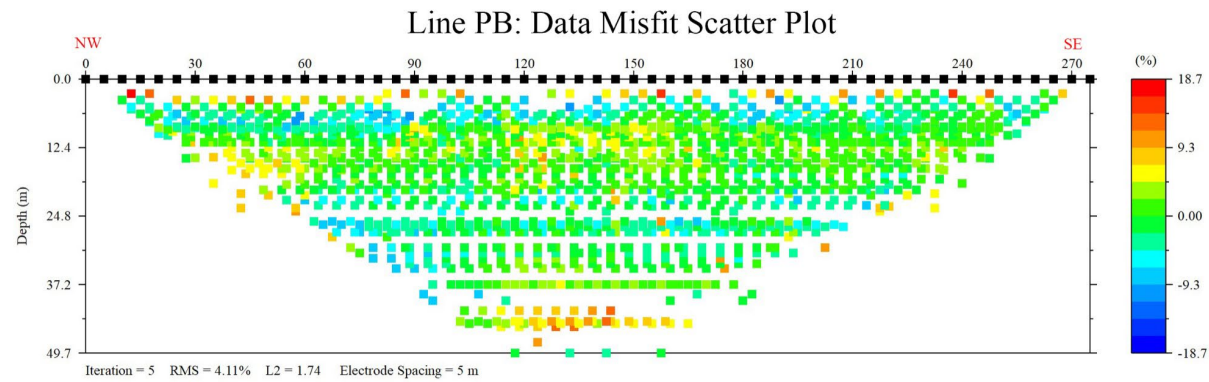


*Figure 5.1-2. The misfit scatter plot measures the error rate between measured and calculated resistivity for Line PB.*

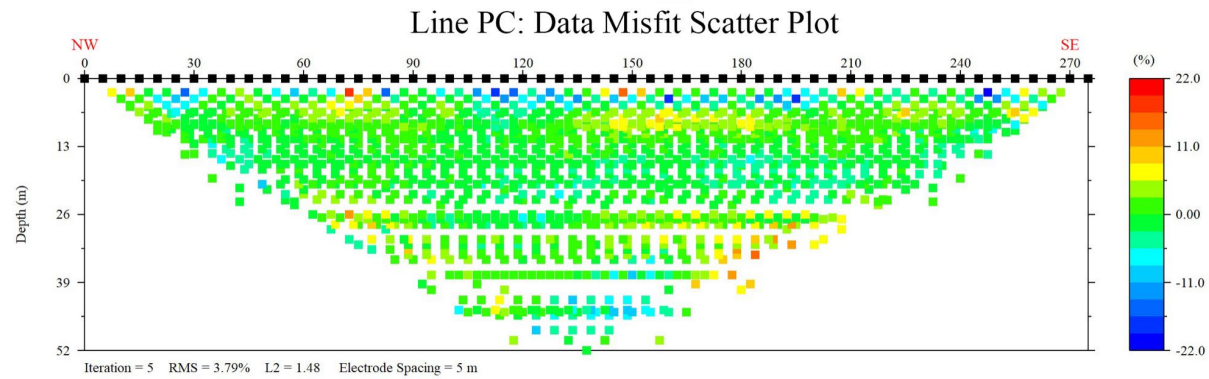


**Figure 5.1-3.** The misfit scatter plot measures the error rate between measured and calculated resistivity for Line PC.

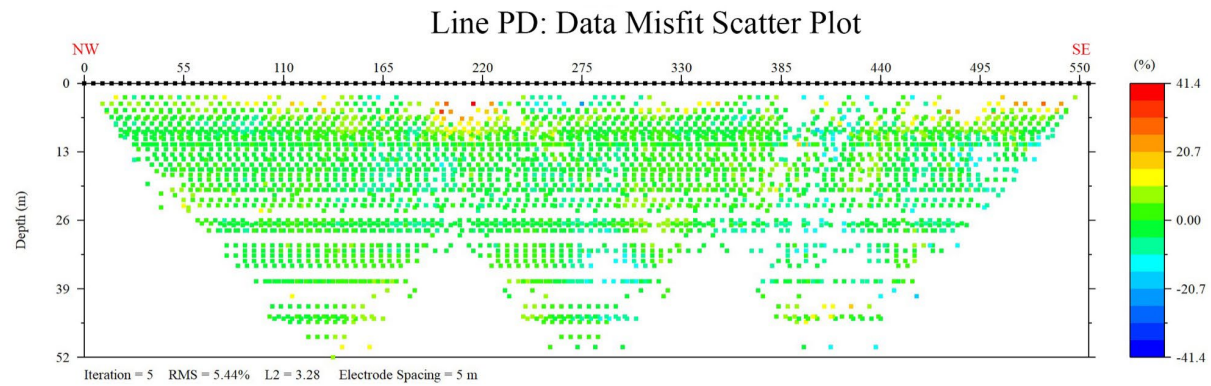


**Figure 5.1-4.** The misfit scatter plot measures the error rate between measured and calculated resistivity for Line PD.

## 5.2 GeoDaze

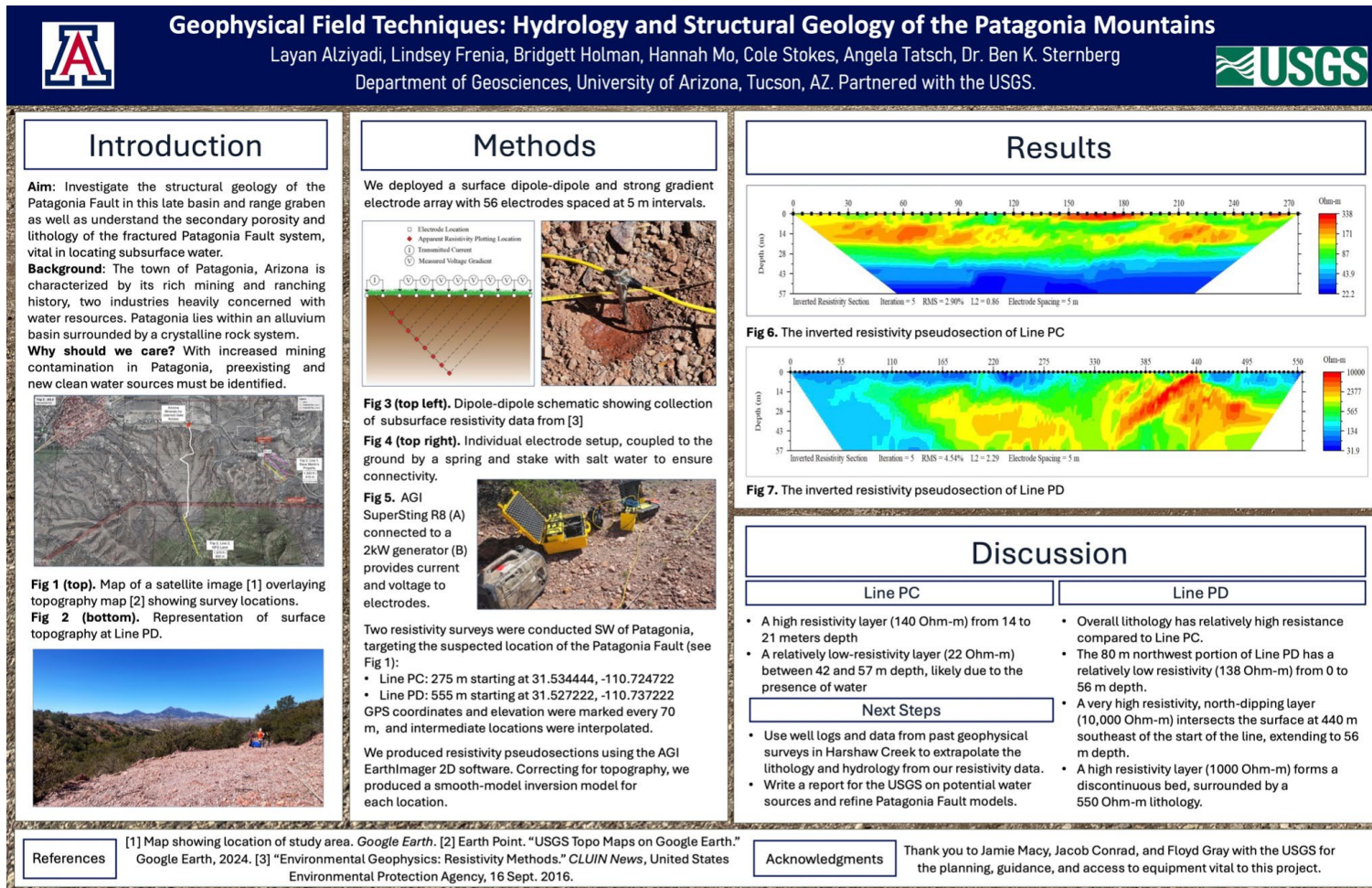
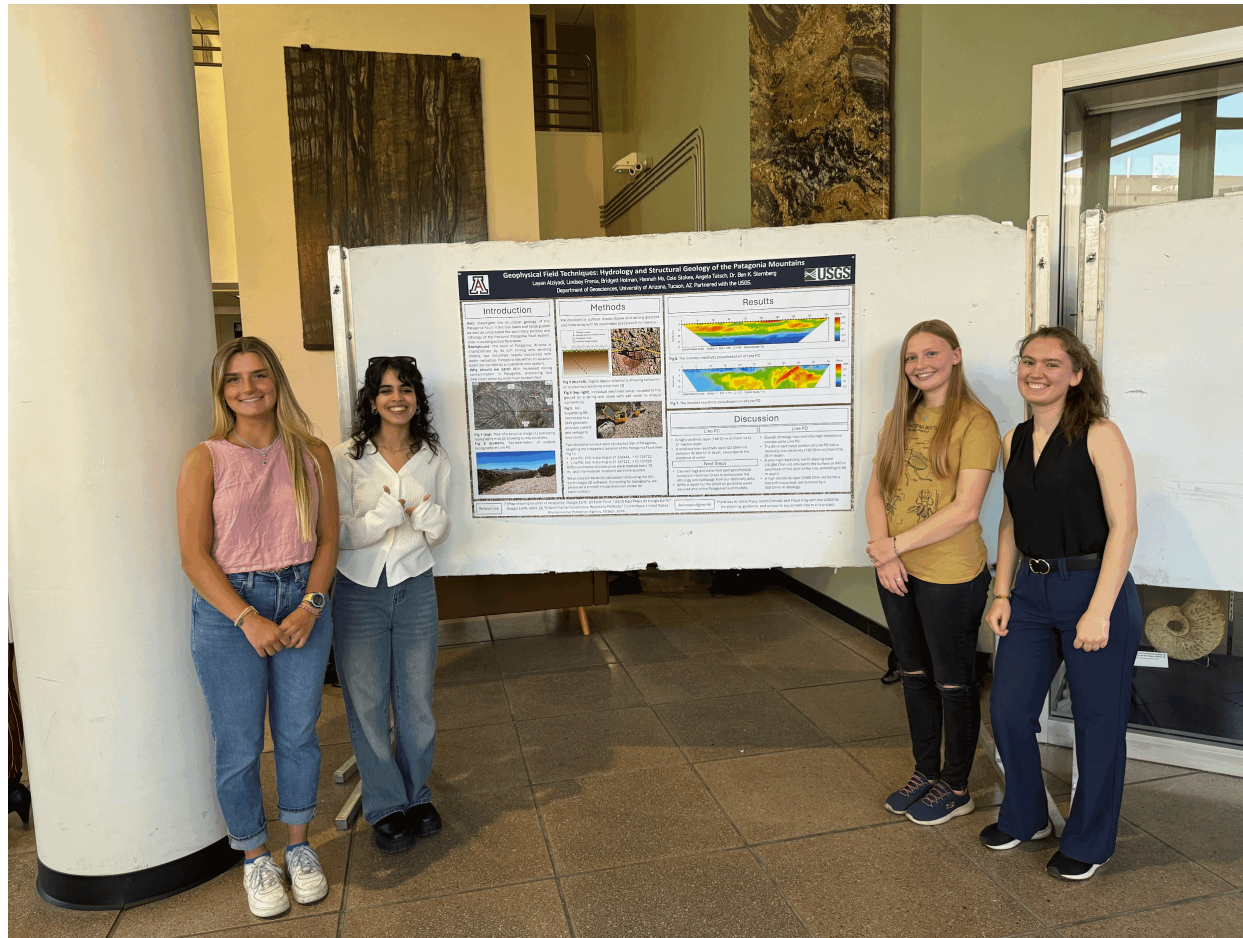


Figure 5.2-1. Poster that was created and presented at the GeoDaze 2024 Student Research Symposium.



*Figure 5.2-2. Picture from the GeoDaze2024 poster presentation.  
From left to right: Lindsey Frenia, Layan Alziyadi, Bridgett Holman, and Angela Tatsch.*

### 5.3 Field Picture



*Figure 5.3-1. Photograph of the class taken in the field on March 2, 2024.  
From left to right: Cole Stokes, Layan Alziyadi, Angela Tatsch, Hannah Mo, Lindsey Frenia,  
Dr. Ben Sternberg, Bridgett Holman, and Jacob Conrad.*

## 6 References

- Alizadeh-Ahlavi, et. al., 2023, Geophysical Surveys in the Harshaw Creek Area, Patagonia Mountains, Arizona, The University of Arizona, p. 33.
- Arizona Geological Survey, 2018, Model of Groundwater Aquifer in the Basin and Range Province: <https://azgs.arizona.edu/photo/model-groundwater-aquifer-basin-and-range-province>
- Choo, H., Burns, S.E., 2014, Review of Archie's equation through theoretical derivation and experimental study on uncoated and hematite coated soils, Journal of Applied Geophysics, v. 105, 2014, p. 225–234, doi:10.1016/j.jappgeo.2014.03.024.
- Dean, S.A., 1982, Acid drainage from abandoned metal mines in the Patagonia Mountains of Southern Arizona. M.S thesis. University of Arizona:  
<http://arizona.openrepository.com/arizona/handle/10150/191766>
- DeCelles, P.G., Ducea, M.N., Kapp, P., and Zandt, G., 2009, Cyclicity in Cordilleran orogenic systems: Nature Geoscience, v. 2, p. 251–257, doi:10.1038/ngeo469
- Hasan, 2019, Dipole-Dipole Array: Electrical Resistivity Methods, Part 3, AGIUSA:  
<https://www.agiusa.com/dipole-dipole%E2%80%8B-%E2%80%8Barray%E2%80%8B>
- South32, Hermosa Project: <https://www.south32.net/what-we-do/our-locations/americas/hermosa>
- Marlow, J.E., 2007, Mining's potential economic impacts in the Santa Rita and Patagonia Mountains region of southeastern Arizona, Sonoran Institute:  
<https://sonoraninstitute.org/files/pdf/minings-potential-economic-impacts-in-the-santa-rita-and-patagonia-mountains-region-of-southeastern-arizona-12012007.pdf>.
- Menges, C.M., 1981, The Sonoita Creek Basin - Implications for late Cenozoic tectonic evolution of basins and ranges in southeastern Arizona: Tucson, University of Arizona, M.S. thesis, p. 239.

## Geophysical Surveys in the Harshaw Creek Area 2024

Mohamad, A.M., Hamada, G.H., 2017, Determination techniques of Archie's parameters: a, m and n in heterogeneous reservoirs, *Journal of Geophysics and Engineering*, v. 14, p. 1358–1367, doi:10.1088/1742-2140/aa805c

Reynolds, M.J., 1997. *An Introduction to Applied and Environmental Geophysics*. Wiley, New York, doi:10.1002/(SICI)1099-0763(199809)5:3%3C179::AID-ARP107%3E3.0.CO;2-2

US Environmental Protection Agency, 2016, Resistivity methods:

[https://archive.epa.gov/esd/archive-geophysics/web/html/resistivity\\_methods.html](https://archive.epa.gov/esd/archive-geophysics/web/html/resistivity_methods.html).

USGS, 1932, Elgin AZ Quadrangle Topographic Map. U.S. Geological Survey, U.S. Department of the Interior: <https://store.usgs.gov/product/527328>

Vikre, P. G., Graybeal, F. T., Fleck, R. J., Barton, M. D., & Seedorff, E., 2014, Succession of Laramide magmatic and magmatic-hydrothermal events in the Patagonia Mountains, Santa Cruz County, Arizona. *Economic Geology*, v. 109, p. 1667–1704, doi:10.2113/econgeo.109.6.1667